Deep-Sea Research II 103 (2014) 79–95

Contents lists available at ScienceDirect

Deep-Sea Research II

journal homepage: www.elsevier.com/locate/dsr2

Investigating the importance of sediment resuspension in *Alexandrium fundyense* cyst population dynamics in the Gulf of Maine

Bradford Butman [a,*], Alfredo L. Aretxabaleta [b], Patrick J. Dickhudt [a], P. Soupy Dalyander [a], Christopher R. Sherwood [a], Donald M. Anderson [c], Bruce A. Keafer [c], Richard P. Signell [a]

[a] U.S. Geological Survey, 384 Woods Hole Road, Woods Hole, MA 02543, USA
[b] Integrated Statistics and U.S. Geological Survey, Woods Hole, MA 02543, USA
[c] Department of Biology, Woods Hole Oceanographic Institution, Woods Hole, MA 02543, USA

ARTICLE INFO

Available online 5 November 2013

Keywords:
Sediment transport
Bottom stress
Sediment resuspension
Harmful algal blooms
Gulf of Maine
Alexandrium fundyense
HAB

ABSTRACT

Cysts of *Alexandrium fundyense*, a dinoflagellate that causes toxic algal blooms in the Gulf of Maine, spend the winter as dormant cells in the upper layer of bottom sediment or the bottom nepheloid layer and germinate in spring to initiate new blooms. Erosion measurements were made on sediment cores collected at seven stations in the Gulf of Maine in the autumn of 2011 to explore if resuspension (by waves and currents) could change the distribution of over-wintering cysts from patterns observed in the previous autumn; or if resuspension could contribute cysts to the water column during spring when cysts are viable. The mass of sediment eroded from the core surface at 0.4 Pa ranged from 0.05 kg m^{-2} near Grand Manan Island, to 0.35 kg m^{-2} in northern Wilkinson Basin. The depth of sediment eroded ranged from about 0.05 mm at a station with sandy sediment at 70 m water depth on the western Maine shelf, to about 1.2 mm in clayey–silt sediment at 250 m water depth in northern Wilkinson Basin. The sediment erodibility measurements were used in a sediment-transport model forced with modeled waves and currents for the period October 1, 2010 to May 31, 2011 to predict resuspension and bed erosion. The simulated spatial distribution and variation of bottom shear stress was controlled by the strength of the semi-diurnal tidal currents, which decrease from east to west along the Maine coast, and oscillatory wave-induced currents, which are strongest in shallow water. Simulations showed occasional sediment resuspension along the central and western Maine coast associated with storms, steady resuspension on the eastern Maine shelf and in the Bay of Fundy associated with tidal currents, no resuspension in northern Wilkinson Basin, and very small resuspension in western Jordan Basin. The sediment response in the model depended primarily on the profile of sediment erodibility, strength and time history of bottom stress, consolidation time scale, and the current in the water column. Based on analysis of wave data from offshore buoys from 1996 to 2012, the number of wave events inducing a bottom shear stress large enough to resuspend sediment at 80 m ranged from 0 to 2 in spring (April and May) and 0 to 10 in winter (October through March). Wave-induced resuspension is unlikely in water greater than about 100 m deep. The observations and model results suggest that a millimeter or so of sediment and associated cysts may be mobilized in both winter and spring, and that the frequency of resuspension will vary interannually. Depending on cyst concentration in the sediment and the vertical distribution in the water column, these events could result in a concentration in the water column of at least 10^4 cysts m^{-3}. In some years, resuspension events could episodically introduce cysts into the water column in spring, where germination is likely to be facilitated at the time of bloom formation. An assessment of the quantitative effects of cyst resuspension on bloom dynamics in any particular year requires more detailed investigation.

Published by Elsevier Ltd.

1. Introduction

Several types of harmful algal blooms (HABs) occur in the Gulf of Maine. The most significant of these are caused by the toxic dinoflagellate *Alexandrium fundyense*,[1] an organism that produces potent neurotoxins that accumulate in shellfish, causing paralytic shellfish poisoning (PSP) in human consumers. The life-history of *A. fundyense* has been described by Anderson and Wall (1978), Anderson (1998), and Anderson et al. (2005c). In brief, blooms

* Corresponding author. Tel.: +1 508 457 2212; fax: +1 508 457 2309.
E-mail address: bbutman@usgs.gov (B. Butman).

[1] In this study, we have focused on the harmful algal species *Alexandrium tamarense* Group I, which we refer to as *A. fundyense*, the renaming proposed by Lilly et al. (2007).

0967-0645/$ - see front matter Published by Elsevier Ltd.
http://dx.doi.org/10.1016/j.dsr2.2013.10.011

begin in spring (April and May) when dormant cysts in the bottom sediments or near-bottom waters (Kirn et al., 2005; Pilskaln et al., 2014b) transition to motile, vegetative cells (germlings) when an internal, annual clock allows them to germinate (Anderson and Keafer, 1987). That germination is further regulated by oxygen, temperature, and light (Anderson, 1980; Anderson et al., 1987). As long as oxygen is present, germination is possible and the rate of germination increases with higher temperature and more light. For example, laboratory studies of germination of cysts from the Gulf of Maine in light increased from 1.6% day^{-1} at 6 °C to 8.7% day^{-1} at 15 °C; at 15 °C in dark conditions, germination was 4.2% day^{-1} (Anderson et al., 2005c). The mechanism(s) by which cysts exit the upper centimeter or so of the bottom sediment has not yet been elucidated. Germination may occur only in a thin, oxygenated veneer at the sediment surface. Cysts buried below that level have insufficient oxygen to germinate and thus will eventually die unless they are moved back to the sediment surface by bioturbation or some other mixing process (Anderson et al., 2014b). *Alexandrium* cysts are thought to remain viable in the sediment for at least a few decades (Keafer et al., 1992).

Once in the water column and depending on conditions such as temperature, light, nutrient availability, and currents, the single-cell germlings can divide and produce vegetative cells that continue to divide asexually to produce blooms, commonly called 'red tides.' Shellfish that ingest sufficient numbers of these cells can become toxic to humans, and their presence requires that the shellfisheries be closed. As blooms subside, the *A. fundyense* cells form cysts that sink to the sea floor and are sequestered in bottom sediment or the benthic nepheloid layer (Kirn et al., 2005; Pilskaln et al., 2014b) over the winter where they remain dormant until the following spring.

Efforts are underway to predict the intensity and extent of *A. fundyense* blooms in the Gulf of Maine, which vary from year to year (McGillicuddy et al., 2005; Anderson et al., 2014b), using coupled physical and biological models (Stock et al., 2005; McGillicuddy et al. 2005, 2011; He et al., 2008; Li et al., 2009). The seasonal prediction strategy uses the distribution of *A. fundyense* cysts in the upper 1 cm of bottom sediment mapped during autumn (a 'cyst map' of the potential seed population) and hydrodynamic model predictions driven by hydrodynamic and atmospheric conditions from past years to form an ensemble of predictions for the current year. During the bloom season, results from an experimental weekly nowcast/forecast system are also available (http://omglnx3.meas.ncsu.edu/GOMTOX/2013forecast/). Results show that the cyst abundance is a first-order predictor of overall modeled bloom severity (He et al., 2008; McGillicuddy et al., 2011). Metrics for characterizing the intensity of blooms include the concentration of the bloom (He et al., 2008; Li et al., 2009), geographic extent of coastline impacted (Kleindinst et al., 2014; Anderson et al., 2014b), and the southernmost extent of coastline closed due to toxicity (McGillicuddy et al., 2011). The model does not include cyst resuspension by currents or waves.

The magnitude of bottom shear stress (tangential force per unit area; hereafter simply stress) caused by the combined action of steady currents and oscillatory wave flow determines sediment (and hence cyst) resuspension. Kirn et al. (2005) observed *A. fundyense* cysts in the water column in the Gulf of Maine and Bay of Fundy in winter and spring, attributed them to resuspension by waves and currents, and proposed that such cysts from resuspension are important in inoculating the spring bloom. This paper extends these ideas by investigating the importance of resuspension and transport in two phases of the *A. fundyense* life history. Two questions are addressed: (1) Are stress events in spring (April and May), when cysts are viable, sufficient to resuspend them from the bottom sediment and mix them into the water column; and (2) can wave- and current-induced resuspension and transport redistribute the dormant cyst population during the winter (October–March), thus altering the distribution of cysts mapped the previous autumn? The answers to both these questions have significant implications for forecasting HABs. For example, if mixing of cysts into bottom water is influenced by stress events, germination might occur episodically rather than at a more constant, gradual rate. Resuspended cysts will germinate more easily in the water column due to the presence of oxygen and possibly light, compared to those in the sediments. If redistribution of the cysts by resuspension occurs after the autumn cyst map data are collected, forecasts might be improved by including this redistribution.

The relationship between the physical forcing (stress) and the sediment response (erodibility) is a key to understanding the mobilization potential of *A. fundyense* cysts. This paper presents estimates of bottom stress in the winter of 2010–2011 and spring of 2011 computed from wave and current models, and field measurements of sediment eroded as a function of stress magnitude at selected locations in the Gulf of Maine. The sediment erodibility observations and stress estimates are used to assess the extent of sediment resuspension and its possible effect on the abundance and germination of *A. fundyense* cysts. Estimates of wave-induced stress for the period 2004–2010 provide an assessment of the inter-annual variability of large stress events.

2. Methods

2.1. Sampling

Sampling of the bottom sediment in the western Gulf of Maine was carried out on two autumn cyst surveys: R.V. *Endeavor* cruise 486 (EN486) from October 10 to 23, 2010 and R.V. *Oceanus* cruise 477 (OC477) from October 23 to November 4, 2011 (Fig. 1). Stations are referenced by letters that refer to their geographic location: Grand Manan (GM), eastern Maine shelf (EMS), central Maine shelf (CMS), western Maine shelf (WMS), central Maine seed bed (CMSB), western Jordan Basin (WJB), and northern Wilkinson Basin (NWB). Although stations are referenced by geographic area for simplicity, they are observations at a single location. The primary objective of these cruises was to map the concentration and distribution of *A. fundyense* cysts in the surficial sediment in autumn to use as the basis for model predictions of blooms the following spring. Samples to determine cyst concentrations and sediment texture were obtained at 101 stations on EN486 and 109 stations on OC477 using a Craib corer with a 0.06-m diameter core barrel that reliably collects cores with undisturbed surface layers (Craib, 1965). Six replicate Craib cores were obtained at stations 43, CMSB, and GM to assess local variability. For cyst analysis, 5 cm^3 of sediment were obtained from the 0 to 1 cm interval of the core and 5 cm^3 from the underlying 1 to 3 cm interval. After sampling for cyst enumeration, there was insufficient sediment left from the 0 to 1 cm sample for texture analysis, so 5 cm^3 of sediment from the 0 to 1 cm interval and 10 cm^3 from the 1 to 3 cm interval were combined, providing a 15 cm^3 sample for texture analysis that characterizes the average texture in the upper 3 cm.

Two 10.7-cm diameter cores were obtained for analysis of sediment erodibility at six locations on EN486 (4, 15, CMS, CMSB, EMS, and GM) and at 10 locations on OC477 (4, 9, WMS, NWB, CMS, CMSB, EMS, 52, WJB, and GM) (Fig. 1) with a U.S. Geological Survey (USGS) hydraulically damped gravity corer designed to collect undisturbed samples of the surficial sediment (Bothner et al., 1997; Law et al., 2008). On OC477, video imagery of the core barrel entering the sediment was obtained at stations in water depths less than 200 m (the pressure limit of the video housing). A qualitative assessment of core quality was based on the video of the core operation; and the extent of edge disturbance, surface

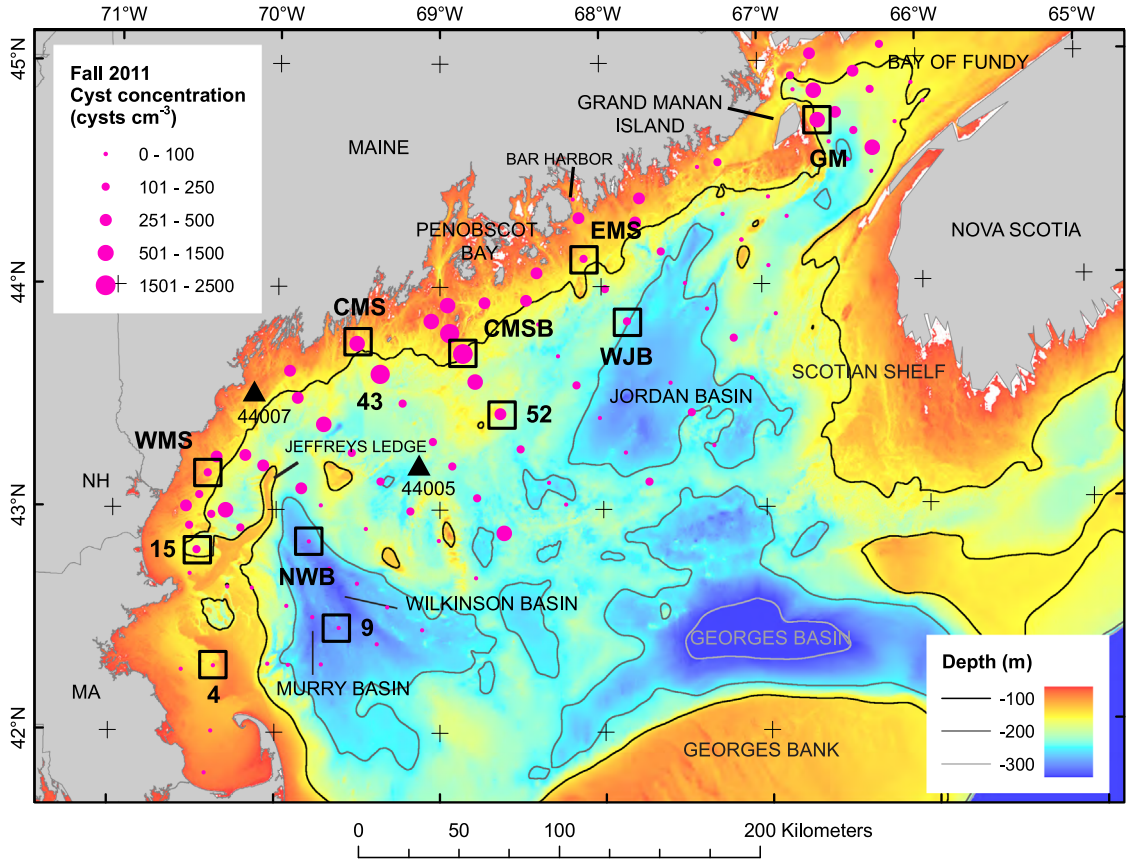

Fig. 1. Stations (Table 1) sampled for erosion analysis (black squares) and concentration of *A. fundyense* cysts in 0–1 cm interval of surface sediment for 2011 (pink circles). Erosion results are reported in this paper for seven stations: Grand Manan (GM), eastern Maine shelf (EMS), central Maine shelf (CMS), western Maine shelf (WMS), central Maine seed bed (CMSB), western Jordan Basin (WJB), and northern Wilkinson Basin (NWB). The surfaces of cores obtained at stations 4, 9, 15, and 52 were deemed disturbed. Samples obtained at the cyst-map stations were analyzed for cyst concentration (0–1 cm and 1–3 cm intervals) and sediment texture (0–3 cm interval). Multiple samples with the Craib corer were obtained at stations 43, CMSB, and GM. Triangles mark locations of NDBC Buoys 44005 and 44007. The largest cyst concentrations are in the Bay of Fundy east of Grand Manan Island (GM); south of Penobscot Bay (CMSB); and southwest along the western Maine and New Hampshire coasts. Isobaths smoothed over ~7 km.

curvature, surface slope, and surface cracking observed in the recovered cores (Fig. 2). The video on OC477 suggested that the core lowering rate used on EN486 could have resulted in cores with disturbed surfaces. Thus, results are reported in this paper only for undisturbed cores collected on OC477 at seven locations (a total of 10 cores): CMSB, GM, EMS, CMS, WMS, NWB, and WJB (Table 1). After processing for erodibility (see Section 2.2), the upper 0–1 cm of the core was extruded and saved for texture analysis.

2.2. Erodibility measurements

Replicate cores from each station collected with the USGS corer were processed onboard to determine the mass eroded as a function of shear stress using a dual core University of Maryland Gust Erosion Microcosm System (UGEMS) manufactured by Green Eyes Environmental Observing Systems (Stevens et al., 2007; Law et al., 2008; Dickhudt et al., 2011). The erosion heads of the UGEMS system used a rotating disc with central suction to impart a nearly uniform, user-specified shear stress to the core surface (Gust and Mueller, 1997). Prior to erosion, sediment cores were extruded so the sediment surface was 0.07 m from the rotating disc of the erosion head. A pump passed 15-μm filtered seawater through the system, generating the central suction and flushing resuspended sediment from the system. The effluent was passed through a bench top turbidity meter to continuously measure the sediment concentration and then collected to calibrate the turbidity meter and determine the number of cysts eroded with the sediment. Each erosion experiment consisted of a sequence of increasing levels of shear stress. The stress levels applied were 0.01, 0.05, 0.1, 0.2, 0.3, 0.45, and 0.6 Pa. The first step (0.01 Pa) was a 30-min flushing step and subsequent steps lasted 20-min. The UGEMS data were analyzed using the erosion formulation of Sanford and Maa (2001). This linear erosion rate expression allows for depth-varying parameters for critical shear stress erosion rate. A variety of devices and protocols have been developed for erosion testing and there is uncertainty in the accuracy and reproducibility of results (Sanford, 2006). One concern is edge effects from the 10-cm diameter UGEMS device, but comparison of results obtained using UGEMS and a Sea Carousel, a 2-m diameter rotating annulus with a 15 cm cross-section (Maa et al., 1993), showed similar erodibility if data were processed in a uniform manner (Sanford, 2006). For a more detailed description of sample processing and data analysis see Dickhudt et al. (2011).

Effluent from one of the two cores collected at each station was used to determine the number of *A. fundyense* cysts eroded at each applied stress level. A subsample (~200 ml) of the effluent from that core and the entire effluent sample from the second core were used for turbidity meter calibration to determine suspended sediment concentration. To prepare the eroded material for analysis of cyst concentrations, the effluent eroded at each stress level was sieved through a 20-μm Nitex screen. The sediment was

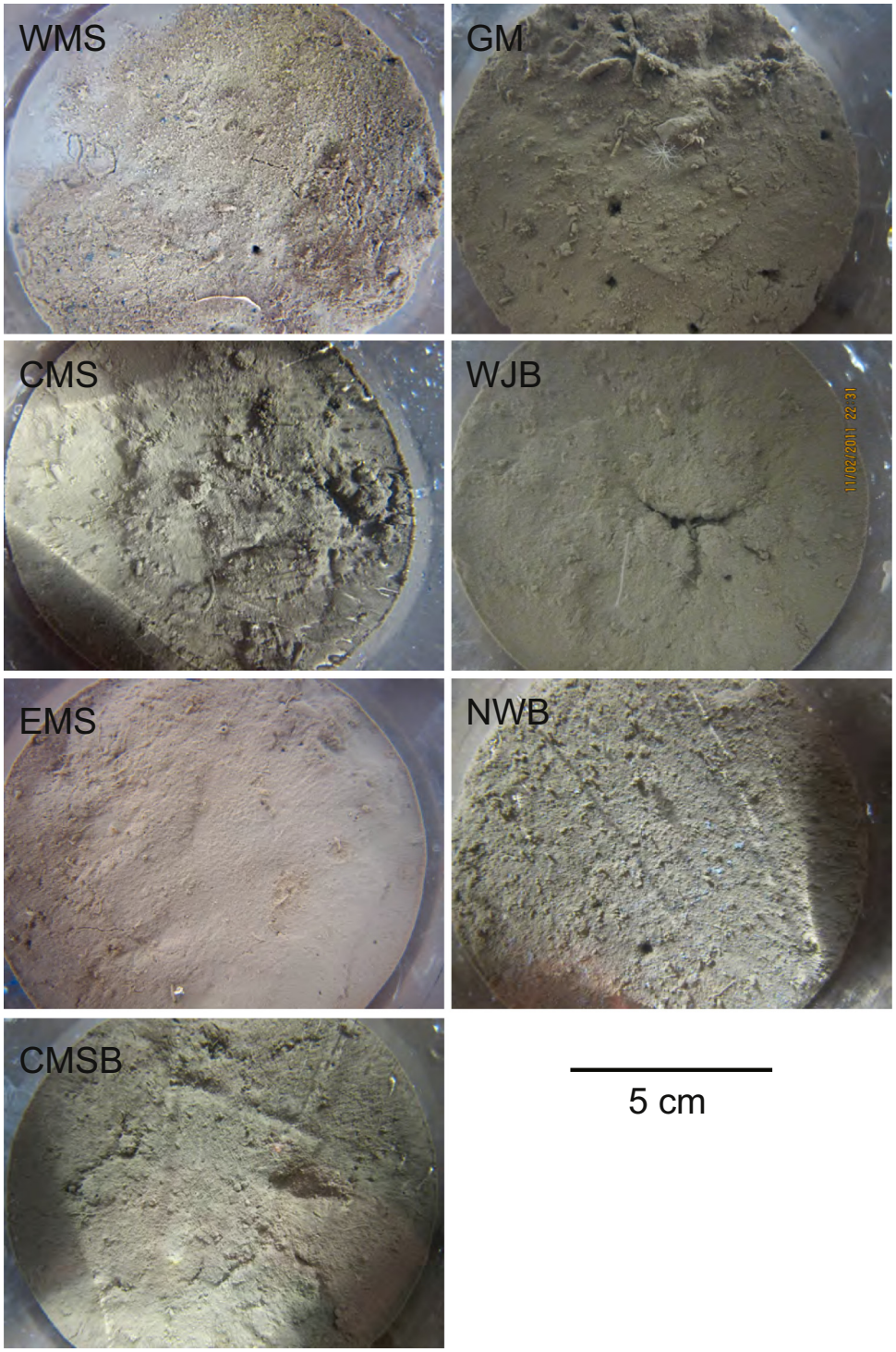

Fig. 2. Photographs of UGEMS core surfaces. Diameter of core tube is 10.7 cm. Uneven lighting (streaks and shadows) reflects conditions on deck when the photographs were obtained.

backwashed into a 50 ml centrifuge tube using filtered seawater, sonicated with a Branson Sonifier 250D at a constant 40-watt output for 1 min, and sieved to yield a clean, 20–100-μm size fraction (Anderson et al., 2003). This sample was preserved by the addition of 0.7 ml of a 20% formaldehyde solution (1% final) and returned to 2–4 °C for at least 24 h. The sample was then centrifuged (3000*g*) for 10 min and the overlying formaldehyde solution removed by aspiration. The resulting pellet was brought up to 10 ml with cold methanol, and stored at −20 °C.

2.3. Sediment texture

The 0–3 cm sample from the Craib cores and the 0–1 cm sample from the UGEMS cores were processed for sediment texture by sieving the sand fraction and using a Coulter counter for the fine fraction, as outlined in Poppe et al. (2000) (Table 2). Solids volume fraction (and concurrently, porosity) was estimated by first determining the solids mass fraction as the ratio of dry weight to wet weight and then converting to volume fraction

Table 1
Location of undisturbed cores obtained in the Gulf of Maine on OC477 in 2011 (Fig. 1).

Station Key	Geographic location	Latitude (N)	Longitude (W)	Water depth (m)	Date sampled	Cyst-map Station
WMS	Western Maine shelf	43.162	−70.421	71	10/26/2011	22
NWB	Northern Wilkinson Basin	42.859	−69.800	265	10/27/2011	29
CMS	Central Maine shelf	43.756	−69.508	95	10/27/2011	42
CMSB	Central Maine seed bed	43.705	−68.860	103	10/28/2011	54
WJB	Western Jordan Basin	43.839	−67.838	201	11/03/2011	71
EMS	Eastern Maine shelf	44.121	−68.104	88	10/29/2011	73
GM	Offshore of Grand Manan Island, Bay of Fundy	44.729	−66.630	122	11/02/2011	97

Table 2
Sediment texture of UGEMS samples (0–1 cm interval following erosion processing) and adjacent Craib cores (0–3 cm interval); cyst concentration in eroded mass; mass eroded at 0.4 Pa; estimate of sediment depth eroded at 0.4 Pa (calculated as eroded mass (in kg m^{-2})/(solids fraction × 2650 kg m^{-3})). Station is the regional identifier (Fig. 1) and the number in parentheses is the cyst-map station, Stdev is standard deviation.

Station	Cruise	Sample	Water depth (m)	Sample depth (cm)	Gravel (%)	Sand (%)	Silt (%)	Clay (%)	Classification	Median (phi)	Mean (phi)	Stdev (phi)	Cysts in eroded material (cysts kg^{-1})	Eroded mass at 0.4 Pa (kg m^{-2})	Solids fraction	Estimated depth of erosion (mm)
WMS	EN486	Craib	72	0–3	0.0	30.9	44.2	24.9	Sand silt clay	6.51	6.11	2.35				
(22)	OC477	Craib	69	0–3	5.8	77.9	12.7	3.7	Sand	1.76	2.25	2.55				
	OC477	UGEMS2	71	0–1	5.2	79.1	11.7	3.9	Sand	1.85	2.37	2.44	1.8×10^6	0.0584	0.42	0.05
NWB	EN486	Craib	226	0–3	0.0	0.3	50.9	48.9	Clayey silt	7.96	7.93	1.4				
(29)	OC477	Craib	246	0–3	0.0	0.1	51.1	48.8	Clayey silt	7.95	7.93	1.33				
	OC477	UGEMS2	254	0–1	0.0	0.3	48.0	51.8	Silty clay	8.05	7.94	1.17	1.3×10^5	0.3500	0.11	1.2
CMS	EN486	Craib	95	0–3	0.0	5.9	64.7	29.3	Clayey silt	7.02	7.04	1.71				
(42)	OC477	Craib	94	0–3	0.0	5.9	55.8	38.3	Clayey silt	7.59	7.52	1.64				
	OC477	UGEMS2	88	0–1	0.0	4.8	58.6	36.6	Clayey silt	7.55	7.46	1.6	3.3×10^6	0.1579	0.11	0.5
CMSB	EN486	Craib	103	0–3	0.0	3.7	62.5	33.7	Clayey silt	7.26	7.23	1.81				
(54)	OC477	Craib	91	0–3	0.0	2.7	58.9	38.4	Clayey silt	7.55	7.56	1.58				
	OC477	UGEMS1	97	0–1	0.0	0.5	59.0	40.5	Clayey silt	7.62	7.67	1.37		0.2039		
	OC477	UGEMS2	87	0–1	0.0	0.6	58.8	40.6	Clayey silt	7.66	7.68	1.36	5.0×10^6	0.1767	0.12	0.6
WJB	EN486	Craib	197	0–3	0.0	7.8	53.9	38.3	Clayey silt	7.55	7.37	1.87				
(71)	OC477	Craib	195	0–3	1.2	16.2	50.4	32.2	Clayey silt	7.12	6.61	2.55				
	OC477	UGEMS3	201	0–1	0.0	5.9	53.1	41.1	Clayey silt	7.67	7.5	1.76	2.3×10^5	0.2704	0.16	0.6
EMS	EN486	Craib	90	0–3	0.0	5.0	64.0	31.0	Clayey silt	7.14	7.15	1.72				
(73)	OC477	Craib	87	0–3	0.0	9.6	57.0	33.4	Clayey silt	7.32	7.12	1.97				
	OC477	UGEMS1	80	0–1	3.4	39.0	35.8	21.9	Sand silt clay	6.09	4.94	3.39	7.4×10^5	0.1606	0.24	0.3
	OC477	UGEMS2	82	0–1	14.9	42.9	27.2	15.1	Gravelly sediment	2.65	3.43	3.91		0.1293		
GM	EN486	Craib	122	0–3	0.0	7.3	53.3	39.4	Clayey silt	7.48	7.32	1.91				
(97)	OC477	Craib	122	0–3	0.0	9.1	57.1	33.8	Clayey silt	7.22	7.13	1.88				
	OC477	UGEMS1	115	0–1	0.2	11.6	56.1	32.1	Clayey silt	7.19	6.97	2.01	1.4×10^6	0.0503	0.22	0.1
	OC477	UGEMS2	118	0–1	0.0	11.7	54.8	33.5	Clayey silt	7.35	7.1	1.92		0.0554		

using a density of water of 1030 kg m^{-3} and a sediment density of 2650 kg m^{-3}. Additional texture data for the Gulf of Maine was obtained from McMullen et al. (2011).

2.4. Cyst concentrations in eroded material

A. fundyense cysts were counted in 1-ml Sedgewick-Rafter slides according to standard methods for cyst identification and enumeration (Anderson et al., 2003) using primulin to stain the cysts (Yamaguchi et al., 1995). The processed and stored samples were centrifuged and aspirated, and 2 ml of primulin stain (2 mg ml^{-1}) was added directly to the sample pellet. After staining for 1 h, the sample was centrifuged and aspirated for the final time and diluted up to 2–10 ml with distilled water, depending on the amount of particulate in the sample. For low stress (levels 1–4), the final resuspension volume was 2 ml and for high stress (levels 5–7), resuspension volumes were 5–10 ml. All *A. fundyense* cysts present in the 1 ml volume of the Sedgewick-Rafter chamber were counted using a Zeiss epi-florescence microscope at 100× with a chlorophyll filter set (excitation band pass 450–490 nm, emission long pass 520 nm). Even though primulin is not a species-specific stain, green-stained "capsule-shaped" cysts representing *A. fundyense* were easily and rapidly counted at low magnification. Some stained *A. fundyense* cysts with no contents may be counted with this method, but these are few in number as empty *A. fundyense* cysts are easily deformed during sonication and sieving and most empty cysts therefore do not have the intact, elongate morphology used as a diagnostic feature for counting. The total number of cysts present in the UGEMS effluent was calculated using the raw cyst count obtained from a 1 ml subsample of the final resuspension volume. The number of counted cysts was standardized to correct for the 200-ml subsample removed for turbidity meter calibration.

2.5. Regional cyst concentrations

Surveys of the cyst concentration in sediment in the Gulf of Maine have been made for 9 years (1997 and 2004–2011; Anderson et al., 2014b). An estimate of the overall distribution was computed by taking the median cyst concentration at each station. Because samples were not obtained at all stations on all

surveys, the number of observations at a station ranged from 1 to 9.

The concentration of cysts kg^{-1} in the 0–3 cm interval at the UGEMS sites was determined using the solids mass fraction of the sample collected for texture analysis, and the concentration of cysts (cysts cm^{-3} wet sediment) in the 0–1 and 1–3 intervals.

2.6. Bottom stress model for 2010–2011

Time-series of wave–current bottom stress (shear stress due to the combined effects of waves and currents) at 1-h intervals for the period October 1, 2010–May 31, 2011 were calculated for the entire Gulf of Maine using modeled currents and waves. Archived modeled currents were obtained from the tidally-resolving Northeast Coastal Ocean Forecast System (NECOFS) which used the Finite Volume Coastal Ocean Model (FVCOM, v3.1.6) (Chen et al., 2003). Hourly values were downloaded from the hindcast archive (http://www.smast.umassd.edu:8080/thredds/archives.html). FVCOM has 40 layers in the vertical and the height of the bottom layer above the sea floor ranged from greater than about 2.5 m in the deep basins to less than 0.5 m on the shelf. Bottom wave orbital velocity and periods were generated using the Simulating Waves Nearshore (SWAN) model (Holthuijsen et al., 1993) and a roughness of 0.05 m, an empirically calibrated model parameter. The currents from the bottom-most layer of FVCOM, the bottom wave orbital velocity and period from SWAN, and a uniform and constant bottom physical roughness of 0.005 m were used for the bed stress calculations following Madsen (1994) (see Dalyander et al., 2012; U.S. Geological Survey, 2012; Dalyander et al., 2013). Harmonic analysis of the FVCOM near-bottom velocities was performed using the MATLAB code t_tide (Pawlowicz et al., 2002) to determine semidiurnal (M_2) tidal strength.

2.7. Sediment resuspension model

The Regional Ocean Modeling System (ROMS) in combination with the Community Sediment Transport Modeling System (CSTMS, Warner et al., 2008) was used to estimate the amount of sediment eroded and the vertical distribution of sediment in the water column during the winter (October 2010–March 2011) and spring (April–May 2011) seasons. CSTMS models sediment response to processes such as erosion, deposition, settling, and bedload transport. The CSTMS implementation used here models bed erosion behavior as a non-cohesive (a property of individual particles) when composed of less than 3% fines (silt plus clay) and as cohesive (a bulk property of the bed) when composed of greater than 20% fines, and used a transitional mixed behavior between 3% and 20% fines. Station WMS was in the transitional behavior and the only station with less than 20% fines (Table 2). For cohesive sediments, the implementation, based on the results of Sanford and Maa (2001) and Sanford (2008), used a linear erosion model with depth varying parameters in the form of $E = M(\tau_b(t) - \tau_c(m))$ where E=erosion rate ($kg\,m^{-2}\,s^{-1}$), M=erosion rate parameter ($kg\,m^{-2}\,s^{-1}\,Pa^{-1}$), $\tau_b(t)$=time varying applied stress (Pa), and $\tau_c(m)$=depth varying critical stress for erosion (Pa). Erodibility of cohesive beds in the model depends on the bulk critical shear stress. The model is initialized with an equilibrium profile that is based on the UGEMS measurements and that typically increases with depth in the bed. The model tracks the bulk critical stress profile as erosion and deposition occur, and models the processes of swelling and consolidation by nudging it toward the equilibrium shape over specified time scales. When erosion occurs, surficial sediment, which tends to have a lower critical shear stress, is removed leaving a less erodible sediment surface. Over time, this over-consolidated material will become more erodible (swell) as the instantaneous critical shear stress profile is nudged toward the equilibrium profile. When deposition occurs, the newly deposited sediment is easy to erode (critical shear stress of 0.05 Pa) but consolidates over time to reestablish the equilibrium profile. For the simulations presented here, swelling time scale was 400 days and the consolidation time scale was 4 days. The consolidation time scale was chosen to be longer than a typical resuspension event but shorter than the expected interval between events. The swelling time scale was chosen to be much longer than a typical resuspension event to minimize the addition of new erodible material during an event. There is very little experimental data to constrain either the consolidation or resuspension time scales but the chosen values are consistent with other studies using a similar bed model (Rinehimer et al., 2008; Sanford, 2008), and simulation results were not sensitive to varying these parameters within a reasonable range.

One-dimensional (vertical) implementations of ROMS were run for each location where sediment data from undisturbed cores were obtained (Fig. 1). Profiles of the critical shear stress for erosion (τ_c) used in the CSTMS model were derived from exponential fits to UGEMS erosion data. A constant value of 0.0005 $kg\,m^{-2}\,s^{-1}\,Pa^{-1}$ was chosen for the erosion rate parameter (M) based on the UGEMS measurements. An analysis following the example in Sanford and Maa (2001) compared the rate of sediment depletion ($M(d\tau_c/dm)$) to the time scale of events for both the UGEMS measurements and the chosen constant value of M. This indicated depth-limited erosion (i.e., erodibility that decreases with depth from the sediment surface) in UGEMS measurements and that the chosen constant value of M would produce depth-limited erosion in the model. The sediment bed initial conditions were obtained from the measured surficial grain size distribution at each site (Table 2). The model internally calculates roughness lengths based on sediment grain roughness, sediment transport, and bedform roughness (*ssw_bbl* formulation described in Warner et al., 2008). The velocity boundary conditions were obtained from the archived FVCOM model run described above; the interior velocity was strongly nudged (adjusted to minimize the difference between the two model solutions with a tendency term that used a one-hour time scale) to approximate the vertical shear from FVCOM. SWAN simulations provided significant wave height and dominant wave period for each location, which were used to approximate the bottom wave orbital velocity assuming a monochromatic wave. Bed changes and sediment concentration in the water column were tracked for three sediment classes that summarize the fractional distribution observed in the cores: one sand class (125 μm) with a settling velocity of 8 $mm\,s^{-1}$ and critical erosion stress of 0.1 Pa; one silt class (mud, 8 μm) and one clay class (mud, 2 μm) both with settling speeds of 0.1 $mm\,s^{-1}$. The sand class was characteristic of the bed material at the study sites; its settling velocity was estimated with the Dietrich formulation (Dietrich, 1982). A settling velocity of 0.1 $mm\,s^{-1}$ was chosen for the mud classes, a value commonly observed in shelf environments and used in sediment transport models (e.g. Hill et al., 2000; Bever et al., 2009; Xu et al., 2011) to represent silt and small flocs. Additionally, 0.1 $mm\,s^{-1}$ is consistent with the observed settling velocity of *A. fundyense* cysts (Anderson et al., 1985) making the behavior of the mud classes representative of both fine sediment and *A. fundyense* cysts.

2.8. Interannual variability in bottom shear stress

The interannual variation in bottom shear stress in the Gulf of Maine depends primarily on waves and storm-driven currents. The interannual variability in the number of wave-driven events that exceed a stress sufficient to mobilize sediment, hereafter referred to as critical erosion stress, was assessed to determine if the primary focus period of this study, 2010–2011, was typical, and to determine an approximate range of variation from 1 year to the

next. A critical erosion stress of 0.1 Pa was chosen for this analysis because this was the minimum applied stress capable of eroding sediment in all cores from the UGEMS erodibility measurements. The longest data records available were wave buoy observations from NOAA buoys 44005 and 44007 (Fig. 1), which cover the time period of 1996-present, with occasional gaps due to instrument malfunction. Neither observed nor modeled current data were available for a sufficient period of time to robustly assess interannual current variability. Given that storm-driven currents are expected to be well-correlated in time with storm-driven waves, the number of wave- and (non-tidal) current-induced events is expected to vary directly with the number of wave-only events. Aretxabaleta et al. (2014) show that the near-bottom currents in the wind band are only a few cm s^{-1}, much less than the tidal currents, and unlikely to contribute to interannual variability in bottom stress.

Wave-induced bottom shear stress was calculated with data from each buoy following Madsen (1994) and using a physical roughness of 0.005 m. Storm-driven events were defined as time periods lasting longer than 6 h when the bottom stress was above 0.1 Pa. Multiple events separated by less than 12 h were assumed to be a single event with a short lull in bottom stress, and were combined into one event (following Butman et al., 2008). Stress using waves from buoy 44007 was calculated at the buoy depth (24 m), whereas stress from buoy 44005 (located in water 206 m deep) was calculated at a shallower depth of 83 m chosen to be representative of shear stress in the central Maine seed bed (CMSB). This method does not account for wave transformation processes that might occur between the two sites to modify the wave field and thus shear stress at a given depth, but should be robust for estimating interannual variability. The number of events was calculated for winter (October–March) and spring (April and May). The years with less than 75% data coverage over the period of interest were excluded.

3. Results

3.1. Regional setting and cyst distribution

The largest and most persistent *A. fundyense* cyst accumulations are found in the Bay of Fundy east of Grand Manan Island and offshore of Penobscot Bay and Casco Bay, Maine (the latter termed the mid-coast Maine seedbed), as summarized in Anderson et al. (2014b) (Fig. 1 and Fig. 3). Cyst concentrations are low in Jordan and Wilkinson Basin.

The bottom sediment texture and M_2 tidal current strength provide an overview of the sea floor environment of the Gulf of Maine and some context for interpreting the cyst distribution (Fig. 3). High-resolution geologic surveys are needed to resolve the complex spatial variability in the surficial geology that occurs in the Gulf; however, the existing data define some broad areas with similar texture characteristics. Along the Maine inner shelf, the sediment texture is varied, with sand, gravel, exposed bed rock, and fine-grained sediment in topographic lows (Barnhardt et al., 1996). Fine silt and clay (median grain size finer than 6 phi (15.6 μm); phi = $-\log_2$(grain diameter in mm)) is found in the northern Gulf of Maine in the region extending northeastward from Jeffreys Ledge to south of Bar Harbor, Maine and offshore about 75 km (Fig. 3A). Jordan Basin is uniformly floored by silt and Wilkinson Basin primarily by clay. The LaHave clay, east of Grand Manan, has been defined on the basis of echograms and texture (Fader et al., 1977) as well as backscatter intensity (Todd et al., 2011; Shaw et al., 2012). Near bottom tidal currents, as defined by the major axis of the M_2 tidal current, are strongest over Georges Bank, the Scotian Shelf, and in the Bay of Fundy; they are weakest in the northwestern portion of the Gulf (northern Wilkinson Basin and along the western Maine and New Hampshire coast) (Fig. 3A). Near-bottom tidal currents are less than 0.1 m s^{-1} on the western side of the Gulf and increase to 0.2–0.4 m s^{-1} on the eastern side. There is a local minimum in the near-bottom tidal flow east and northeast of Grand Manan, associated with a minimum in mean kinetic energy (Greenberg, 1979) and a minimum in eddy viscosity (Lynch and Naimie, 1993). The amplitude of the M_2 minor axis, a measure of the minimum tidal current flow, is less than 0.05 m s^{-1} over most of the Gulf of Maine, except over Jordan Basin and the region leading to the Bay of Fundy (Fig. 3B).

Sediment texture at the UGEMS sites was consistent with the overall sediment distribution in the Gulf of Maine. Sediment was clayey silt at CMS, CMSB, WJB, NWB, and GM; sand at WMS; and a mix of gravel, sand and fines at EMS (Table 2). The size-class fractions determined from the Craib cores at regional stations on EN486 and OC477 and from the UGEMS cores typically agreed to within a few percent, except at EMS where the Craib sample obtained on OC477, separated by about 200 m, was significantly finer than the UGEMS sample.

3.2. Sediment erodibility

The UGEMS results provided estimates of the mass of sediment eroded as a function of applied shear stress (Fig. 4, Table 2). At all stations, erosion began between 0.05 Pa and 0.1 Pa; thereafter, the rate varied depending on location. The mass eroded for a given applied stress was largest at the basin stations NWB (265 m water depth) and WJB (200 m), where sediments were silt and clay; and smallest on the WMS (71 m), where sediment was sandy, and GM (122 m) in the Bay of Fundy where the sediment was clayey silt. The mass eroded increased with increasing water depth (Table 2), with the exception of GM. Using the measured porosity of the UGEMS samples and the eroded mass at 0.4 Pa, approximately 1.2 mm of sediment was eroded from the core obtained in NWB and less than 0.7 mm at all other stations. Mass eroded for the replicate cores obtained at CMSB, WMS, and GM, where both cores were undisturbed, was similar. The mass eroded at 0.4 Pa increased linearly with increasing clay-to-silt ratio (Fig. 5), except at GM, where the sediment was the least erodible of all tested.

3.3. Bottom stress

The value of wave–current stress exceeded 5% of the time, a measure of the largest stresses, decreases from east to west across the central Gulf of Maine (Fig. 6) reflecting the strength of the near-bottom tidal current (Fig. 3), and increases in water less than about 100 m deep reflecting the contribution of surface waves. The weakest stresses (less than 0.05 Pa 95% of the time) occur in the northwest portion of the Gulf (offshore of southern Maine and New Hampshire) in water deeper than 100 m where tidal currents are weakest and wave-driven currents do not significantly reach the sea floor. Bottom stress caused by waves is minimal in the Bay of Fundy because of the limited fetch that produces shorter period wind-waves that do not reach as deeply as longer period swell. The spatial pattern of the value of stress exceeded 5% of the time (Fig. 6) was similar between winter and spring (not shown), reflecting the dominance of tidal currents driving the stress. However, the stress exceeded 5% of the time in winter was slightly greater than in spring in shallower water along the Maine-New Hampshire-Massachusetts coast, over the isolated topographic highs in the Gulf of Maine, and on Georges Bank reflecting additional wave events in winter (Table 3). In Jordan Basin, the stress exceeded 5% of the time was less than 0.1 Pa on the western side of the basin, where station WJB was located, and increased to 0.1–0.2 Pa toward the east. In Wilkinson Basin, stress exceeded 5%

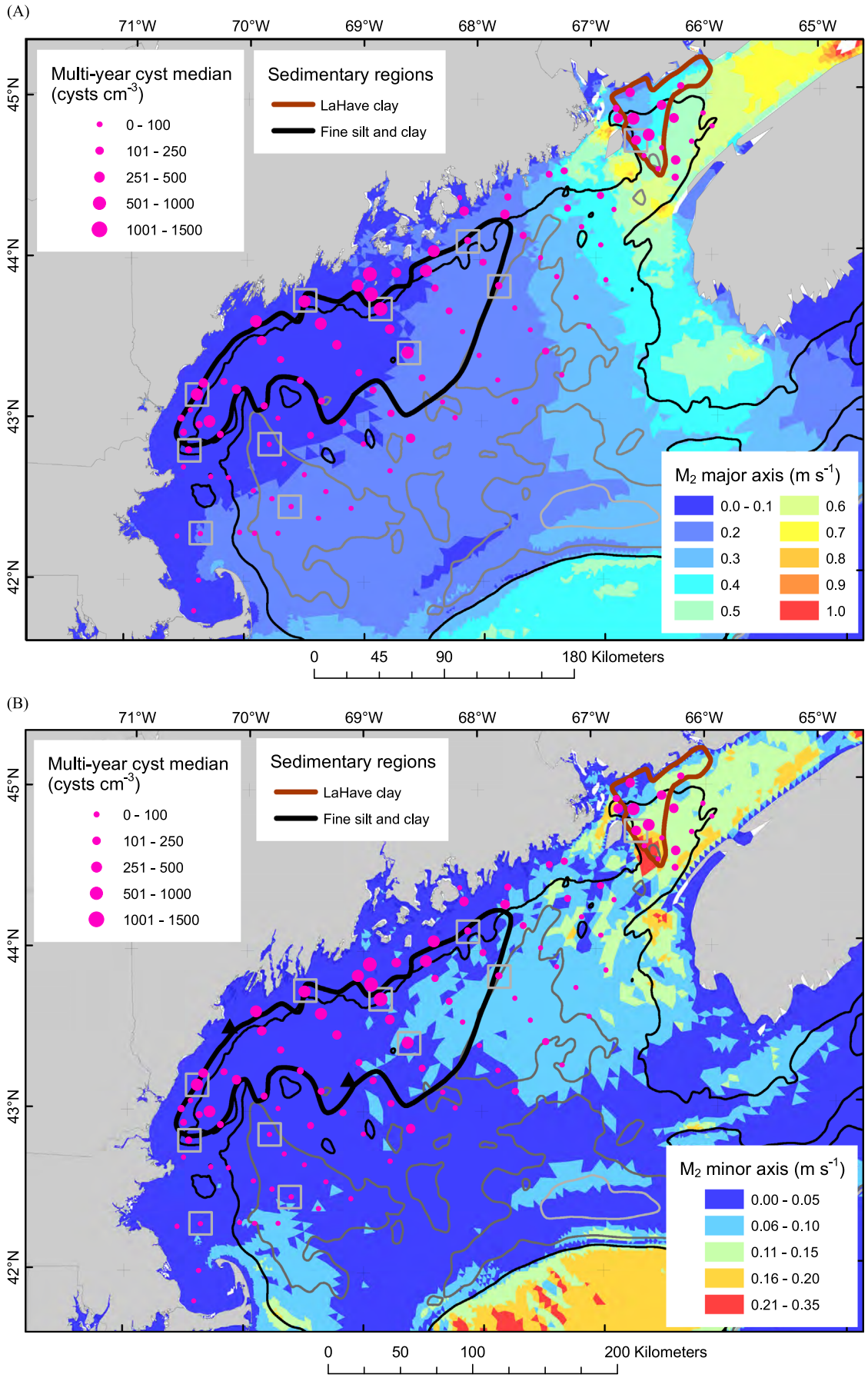

Fig. 3. (A) Amplitude of the major axis of the bottom M_2 tidal current (computed from FVCOM forecast data), polygons outlining the sedimentary regions of fine silt and clay (6–10 phi) and the LaHave clay; and the median of the *A. fundyense* cyst concentration in 0–1 cm interval for 2004–2011 regional surveys (Anderson et al., 2014b). The smoothed 100-m isobath is in black and smoothed 200 and 300 m isobaths are in gray and light gray, respectively. (B) Amplitude of the minor axis of the bottom M_2 tidal current (a measure of the minimum bottom current); sedimentary regions and cyst concentration as in (A). Gray squares outline UGEMS stations. Note different current speed scales in A and B.

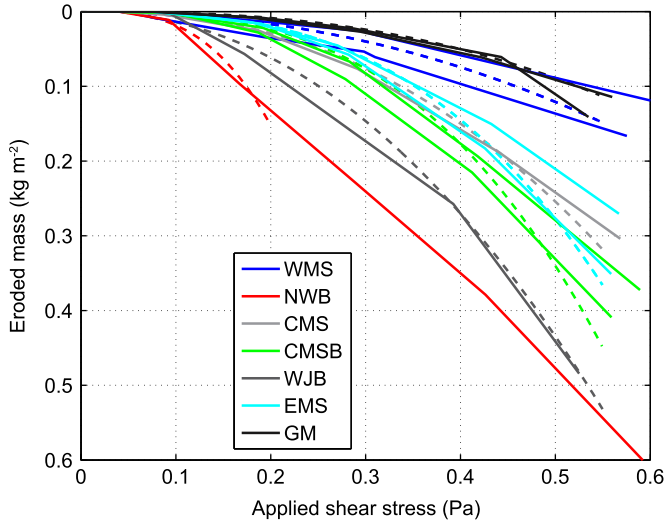

Fig. 4. Eroded mass vs. applied stress for undisturbed cores (all obtained on OC477) (solid lines). Replicates are shown for stations GM, EMS, and CMSB where both cores were deemed undisturbed. Dashed lines show exponential fits for erosion simulations using the Community Sediment Transport Modeling System (CSTMS).

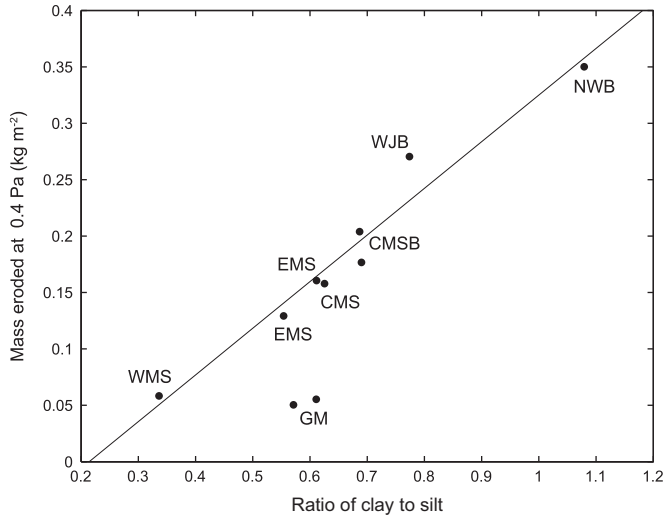

Fig. 5. Eroded mass at 0.4 Pa vs. ratio of clay to silt in 0–1 cm interval of UGEMS core (sampled after erosion measurements). Linear fit (with GM data excluded) is: Mass Eroded at 0.4 Pa = 0.41(ratio of clay to silt)–0.09; $R^2 = 0.89$.

of the time was < 0.05 Pa in the northern basin in vicinity of station NWB, increasing to 0.05–0.1 Pa to the south.

The strength and variability of the near-bottom combined wave–current stresses calculated following Madsen (1994) (using a MATLAB implementation of the Soulsby (1997) formulation) at each of the study sites reflects the increase in tidal currents to the east and decrease in wave stress with water depth (Fig. 7). At the shelf stations (WMS, CMS, EMS, and GM), the persistent bottom stress caused by tidal currents was weakest at WMS and largest at GM, where tidal stress exceeded 0.4 Pa. At WMS, the bottom stress was mostly less than 0.1 Pa, but exceeded 0.4 Pa during a few storm events. At CMSB, in the central Maine seedbed, tidal currents contributed a small but significant stress of $\sim$0.05 Pa to the stress time-series, and stress exceeded 0.4 Pa during one storm event. At GM in the Bay of Fundy, offshore of Grand Manan, the dominant stress was from the strong tidal currents and there was spring-neap modulation of about 0.15 Pa; wave stress during large storms was minor, as this location is partially shielded from waves associated with nor'easters. In the deep basins, the bottom stress was mostly less than 0.1 Pa (WJB) and less than 0.05 Pa (NWB), and dominated by tidal currents with no contributions from surface waves.

The number of events where the wave current-stress exceeded 0.1 Pa at buoy 44007 for winter 2010–2011 and spring 2011 was slightly above average (within one standard deviation) for the time period of 1996–2011 (Table 3). At the deeper location (buoy 44005), the number of events in the 2010–2011 period was slightly below average compared to the rest of 1996–2012, but was within one standard deviation. At buoy 44005 (buoy at 206 m, wave stress calculated at 83 m), the number of resuspension events ranged from 0 to 10 in winter (6 months) and 0–2 in spring (2 months); at buoy 44007 (24 m) the number of resuspension events ranged from 11 to 23 in winter and 1–8 in spring (Table 3).

3.4. Sediment resuspension

The modeled time series of suspended sediment concentration in the water column during winter–spring 2010–2011 (Fig. 7) reflects the magnitude and duration of energetic stresses, the composition of the bed, the erodibility of the bed, the sequence of resuspension events that alter the erodibility profile and the sediments at the surface of the bed, and the vertical velocity and stratification in the water column (in FVCOM). The model estimates of sediment resuspension can be grouped based on frequency and extent of resuspension, and the processes causing resuspension. The tidal current provided a consistent background stress that decreased from east to west and offshore, and was strongest at GM. The model predicted near constant mobility at GM and EMS, primarily as a result of the tidal currents. At CMS, CMSB, and WMS, resuspension was episodic caused by wave–driven currents associated with storms; the largest two storms during the simulated period occurred in late December 2010 and mid-April 2011. Variability in the stress between stations partially reflects the spatial variability in the wind and wave field. In the deep basins, where the tides are weak and the water is too deep for wave currents to affect the sea floor, the model predicted very small resuspension at WJB and no resuspension at NWB. The modeled sediment concentrations of the two mud classes (silt and clay) in the water column greatly exceeded those for the sand class because of their smaller settling velocity and the larger mud fraction in the surface sediments, typically greater than 90%, except at EMS and WMS where the sediment was about 40% and 80% sand, respectively.

At GM (122 m water depth) the stress was dominated by tidal fluctuations at semidiurnal frequencies modulated at the spring-neap period (Fig. 7). The critical erosion stress for both sand (0.1 Pa) and recently-deposited mud (0.05 Pa) and was exceeded most of the time, causing the eroded mass to gradually reach equilibrium within about 3 months from the beginning of the simulation. Sediment remained suspended for most of the simulated period until late April when the stress dropped below the threshold value. Maximum sand concentrations were associated with periods of spring tides, but the magnitudes were very small.

At EMS (88 m water depth) both wave and tidal stresses were important (Fig. 7). A series of storms, superimposed on a background tidal stress of about 0.1 Pa, gradually eroded the bed about 0.5 mm. The difference between the critical erosion stress for mud and for sand is a key determining factor for the sediment evolution at EMS, because when only the mud threshold was exceeded, mud remained in resuspension (resulting in a near-constant eroded mass) while sand was able to redeposit in the bed (resulting in eroded mass more event driven). The constant cycles of resuspension and deposition caused the modeled instantaneous critical stress profiles to evolve to be more erodible than the equilibrium

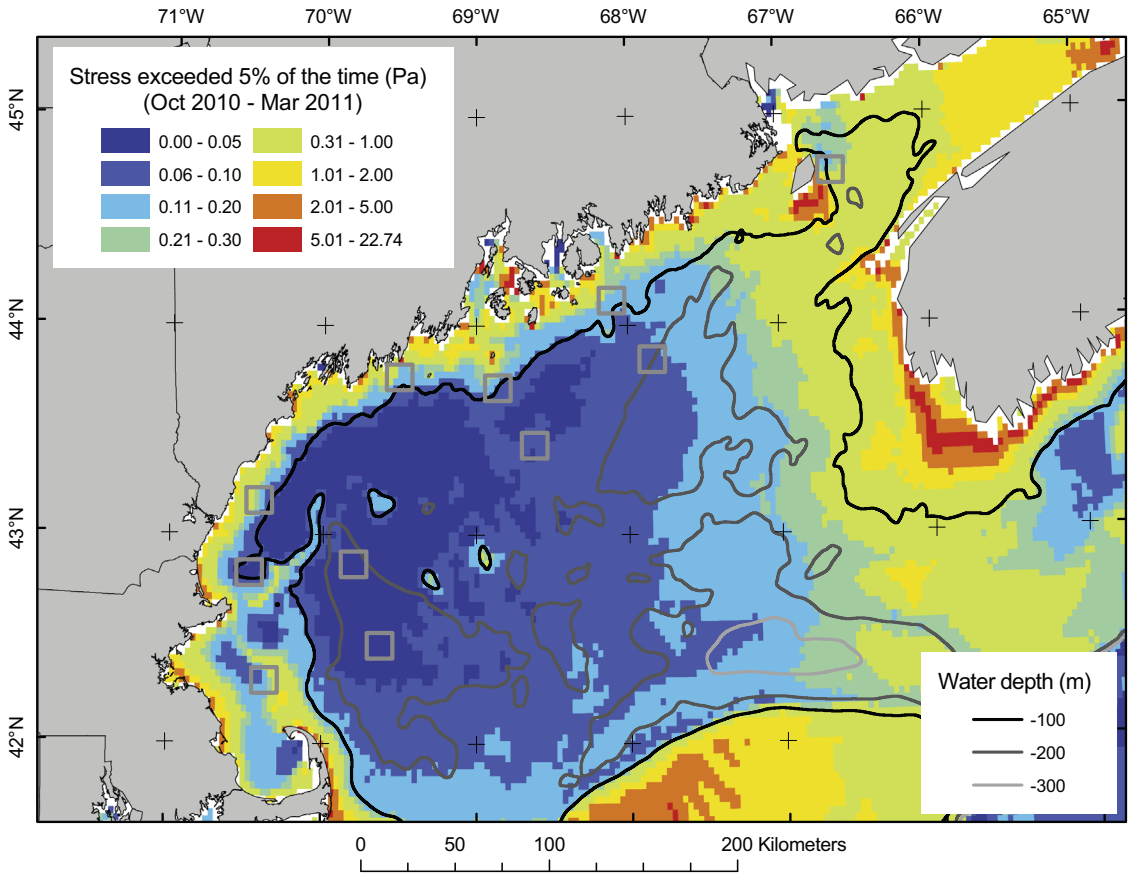

Fig. 6. Value of wave–current bottom stress exceeded 5% of the time for winter (October 2010–March 2011). The stress decreases from northeast to southwest, reflecting the strength of near-bottom tidal currents (Fig. 3), and increases along the coast in water depths less than 100 m, reflecting the effect of surface waves. The pattern in spring (not shown) is similar. Gray squares outline UGEMS stations.

Table 3
Number of events when the wave-induced bottom shear stress exceeded 0.1 Pa for greater than 6 h based on buoy observations between 1996 and 2011. Winter is defined as October through March; spring is April and May. Included is the depth of calculation, the number of years with sufficient data coverage for inclusion, the mean value, the standard deviation (St. Dev.), the range, and the value for the 2010–2011 time period focused on in this study.

Buoy	Season	Depth (m)	Years	Mean	St. Dev.	Range	2010–2011
44007	Winter	24	13	17.5	3.3	12–23	20
44005	Winter	83	9	5.8	3.1	0–11	4
44007	Spring	24	14	5.0	2.0	1–8	6
44005	Spring	83	10	0.6	0.7	0–2	1

profile (Fig. 4), resulting in high resuspension volumes. The mass of suspended sediment that corresponded to sand was largest at EMS because of the higher percentage of sand, relatively large stresses, and easily eroded material (Fig. 4). There was more suspended sediment at EMS than at any other station, but the maximum eroded depth was larger at CMS and CMSB which had higher porosity than EMS (Table 2).

At CMS (95 m water depth), the December storm eroded about 1.5 mm of sediment, and two subsequent smaller storms kept sediment in suspension for more than a month. A mid-December and mid-April storm both eroded about 0.7 mm, but the vertical extent of the suspended sediment was limited by the vertical distribution of velocity and turbulence in the model (largely constrained by the flow and stratification in FVCOM), resulting in the sediment settling to the bed within a few days. Reduced mixing or strong downwelling limited the vertical extent of the sediment resuspension in the water column.

At CMSB (103 m water depth) sediment resuspension was dominated by a single storm event at the end of December 2010 (Fig. 7). The model predicts about 1 mm of the bed was eroded during this event, and the suspended material took about 2 weeks to settle and return to background. The sediment resuspended during this storm event is estimated to mix vertically over the entire water column with larger concentrations in the first few meters above bottom (Fig. 8). There is a delay between the peak stress and the maximum suspended sediment in the water column, as sediment continues to be eroded until the stress falls below threshold. Sediment, especially mud, can remain suspended for long periods of time when bottom stress remains above the erosion threshold (for example, at EMS and GM, Fig. 7).

At NWB, the simulated stress never exceeded threshold. At WJB the stress, caused by primarily by tidal currents, was almost always less than 0.1 Pa. Stress exceeded 0.1 Pa in December and April during two storms coincident with spring tides, causing small resuspension (not visible at the scale shown in Fig. 7).

The maximum eroded depth during the winter–spring period (Figs. 9 and 10A), an estimate of the maximum perturbed layer in the bed, exceeded about 0.5 mm at stations shallower than 140-m water depth, except at WMS, where the higher fraction of coarser sediment resulted in maximum eroded depths of order 0.2 mm. There was little or no sediment mobility at stations sampled deeper than 200 m; resuspension in western Jordan Basin was negligible (maximum eroded depth of 0.01 mm) and the model did not calculate any resuspension in northern Wilkinson Basin. The estimated maximum eroded depth in the central Maine seed bed

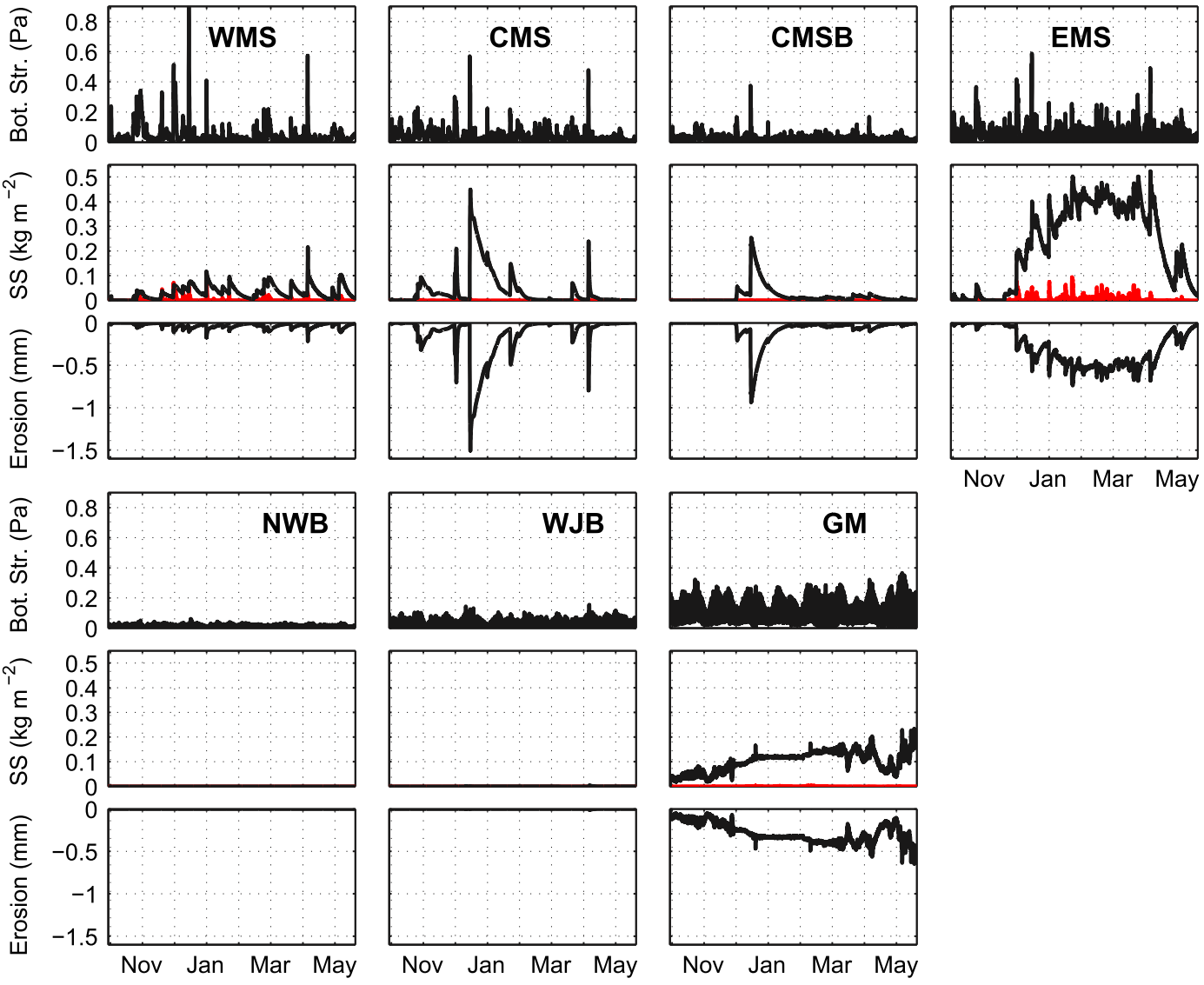

Fig. 7. Results of the resuspension simulation at WMS, CMS, CMSB, EMS, NWB, WJB, and GM for the period October 1, 2010–May 31, 2011. For each station, the top row shows the time series of wave–current bottom stress; the second row shows the integrated suspended sediment (SS) in the water column for sand (125 μm) (red) and for mud (2 and 8 μm) (black); and the bottom row shows the eroded depth. Month labels and grid correspond to mid-month (day 15 of each month). To obtain average suspended concentration in the water column in mg l^{-1} assuming mass is distributed uniformly, multiply SS by 1000/water depth (m).

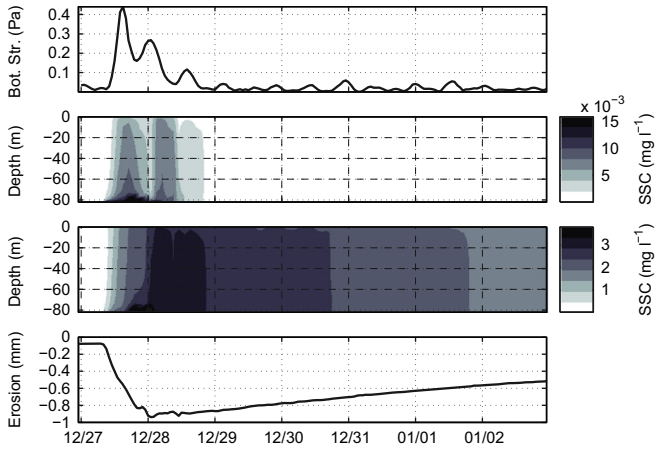

Fig. 8. Time series of wave-current bottom stress (top panel); integrated suspended sediment concentration for sand (125 μm) (second panel) and mud (2 and 8 μm) (third panel); and eroded depth (bottom panel) at station CMSB for the December 27–28, 2010 event.

(CMSB) was about 1.0 mm and occurred during the late December storm. Despite the persistent tidal stresses in the Bay of Fundy (Fig. 7), the maximum eroded depth was about 0.6 mm because of the low erodibility of the sediment in this region (Fig. 4). The mean eroded depth (Figs. 9 and 10B), the average of the eroded depth over the winter–spring period and a measure of the average amount of bed material in suspension, was largest at EMS and GM, a result of the persistent tidal currents that maintained a near-constant 0.5 mm of sediment in suspension once steady state was reached (Fig. 7). The mean eroded depth at the stations in water depth less than 120 m ranged from approximately 0.05 to 0.2 mm. The smallest mean eroded depths are estimated for stations in water depths greater than about 120 m, and at WMS.

Both maximum eroded depth and mean eroded depth generally increased with maximum wave–current stress (Fig. 10), with the coarse sediment station WMS an outlier. Stations GM and EMS, and CMSB and CMS have similar maximum bottom stresses, but the maximum eroded depth was higher for CMSB and CMS because they have a higher erosion rate (Table 2). However, the mean eroded depth was higher at GM and EMS where the persistent tidal currents

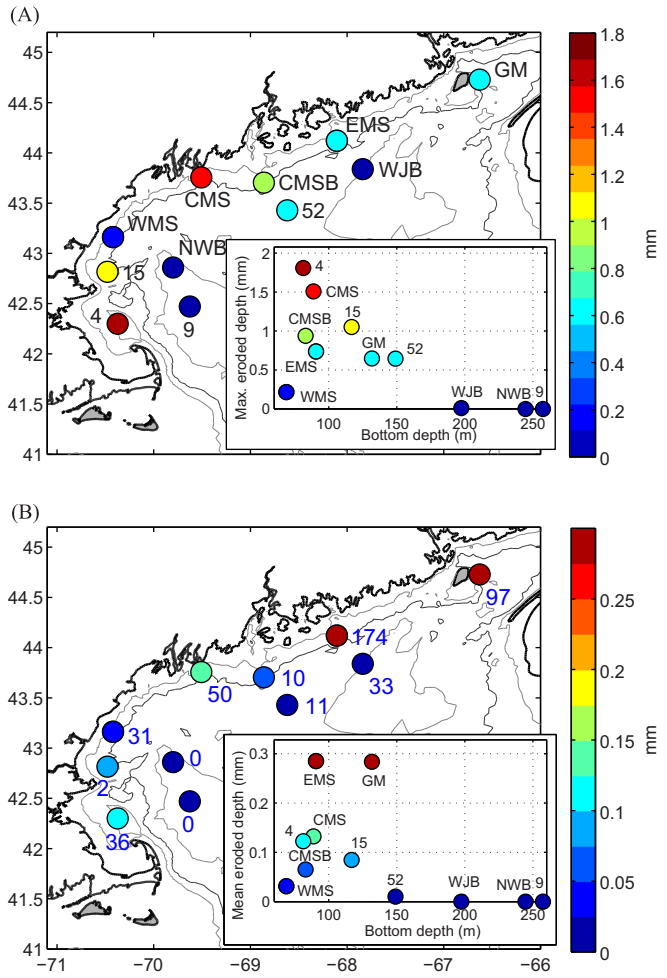

Fig. 9. (A) Maximum depth of sediment eroded and (B) mean eroded depth during resuspension simulation for the period October 1, 2010–May 31, 2011. Both (A) and (B) show parameters in map view and as a function of bottom depth (inset graph lower right). See Fig. 1 for station key. The number adjacent to the stations in (B) is the number of times the threshold of 0.1 Pa is exceeded. Although stress exceeds the threshold each tidal cycle at GM (northernmost station), the number of events is limited by the 6 h persistency requirement for an event. Isobaths are 50, 100 (dark) and 200 m. The mean eroded depth over the winter-spring period is a measure of the average amount of bed material in suspension.

maintain sediment in suspension for most of the simulated period (Fig. 7).

4. Discussion

The largest cyst populations in the Gulf of Maine generally are found in the area of fine silt and clay and M_2 tidal currents less than about 0.10 m s^{-1} (Fig. 3). The minor axis of the M_2 tidal current (Fig. 3B) is a measure of the weakest current that occurs at a particular location, and sets an approximate threshold for passive particle settlement. In the Gulf of Maine (excluding the Bay of Fundy), cysts were found in regions where the minor axis of the tidal current was less than 0.10 m s^{-1} (Fig. 3B and Fig. 11), and mostly less than about 0.07 m s^{-1}. Near-bottom current speeds less than this value appear necessary for cysts, where present, to become incorporated into the sediments. However, there are regions where the minimum tidal current is less than 0.10 m s^{-1} and cysts are not found in abundance, suggesting that incorporation of cysts into the sediment in these regions is also limited by the dynamics of the bloom and the regional circulation (McGillicuddy et al., 2005; Anderson et al. 2014).

The area of high cyst concentration northeast of Grand Manan Island is in a local minimum of the M_2 current. In addition, sediment at GM was unique compared to the sediments at stations in the Gulf of Maine. GM sediment was the most difficult to erode (Fig. 4), fell below the mass-eroded vs. clay-to-silt ratio curve defined by the other UGEMS stations in the Gulf of Maine (Fig. 5), and was an outlier in the mean eroded depth vs. water depth (Fig. 9) and mean eroded depth vs. wave stress (Fig. 10) curves. Station GM, and the high cyst concentrations in the region east and north of Grand Manan, are in a triangle-shaped, fine-grained sedimentary environment east of Grand Manan extending northward toward the St. John River (Fig. 3) (Martin et al., 2014). This region of seabed is identified as LaHave clay (Fader et al., 1977; Fig. 3), and defined as a muddy seascape on the basis of multibeam bathymetry and backscatter and other characteristics (Shaw et al., 2012). These sediments are most likely derived from winnowing of glacial till on the floor of the Bay of Fundy during the last rise in sea level, as well as some contribution from the Saint John River (Fader et al., 1977). The deposit is located in a local minimum of bottom tidal currents (Fig. 3), bottom stress (Fig. 6), and Sediment Mobility Index. The Sediment Mobility Index is a parameter that integrates both magnitude and frequency of sediment mobilization and is defined as: τ/τ_{cr} times the percentage of time τ_{cr} is exceeded, where τ is bed shear stress and τ_{cr} is critical bed stress (Shaw et al., 2012). This area is described as having an 'active surface layer and immobile compact substrate under present tidal conditions' (Shaw et al., 2012). The resistance of the LaHave clay to erosion, the local minimum in stress, and a persistent residual counter-clockwise gyre (Aretxabaleta et al., 2008) are unique features of this region of high cyst abundance.

The clay to silt ratio is representative of the grain size distribution in the fine sediment fraction and may be related to bed erodibility (van Rijn, 2007; Dickhudt et al., 2011; Le Hir et al., 2011). In some cases, an increase in the clay to silt ratio may cause a muddy bed to become more cohesive and less erodible. Alternatively, an increase in the clay to silt ratio may inhibit dewatering and result in a less consolidated and more erodible bed. The UGEMS mass eroded at 0.4 Pa increased linearly with the clay to silt ratio in the Gulf of Maine (Fig. 5). While this may imply that the effect of inhibited consolidation outweighed increased cohesiveness (in fact solids fraction does decrease as clay to silt ratio increases, not shown), the relationship between erodibility and solids fraction (not shown) was not as strong as that with clay to silt ratio implying other unaccounted for factors. While the relationship between clay to silt ratio and erodibility is not directly causative, it is quite strong ($R^2=0.89$) and this relationship was used to predict erodibility at other locations (Figs. 9 and 10) where the surface of the UGEMS cores was deemed disturbed. Further UGEMS observations would be helpful to evaluate the robustness of the eroded-mass to clay-to-silt ratio relationship and its suitability to estimate erodibility in model simulations of sediment resuspension where texture data are available.

Collecting quality cores for erosion analysis in deep water proved difficult; only 10 cores obtained at seven different stations on OC477 had an undisturbed sediment surface (Table 2). Almost all cores on both cruises were recovered with clear water above the sediment-water interface, suggesting cores undisturbed in the coring process. However, despite overlying clear water, the surfaces of some cores were rounded, sediment was pulled away from the core tube around the edges, or the surface was cracked. Interestingly, the mass eroded from all cores using the UGEMS system fell approximately in the same range, whether their surfaces were determined to be disturbed or undisturbed. However, the relationship between erodibility and the clay-to-silt ratio (Fig. 5) was only well-defined for the undisturbed cores.

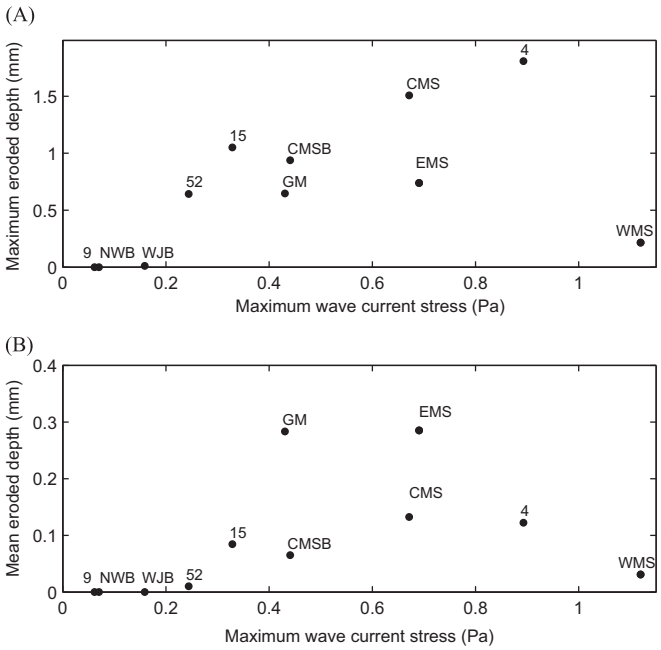

Fig. 10. (A) Maximum eroded depth and (B) mean eroded depth as a function of maximum wave-current stress for the period October 1, 2010–May 31, 2011. Stations identified by numbers are locations where the surface of cores were determined to be disturbed; at these locations the erosion rate curve was determined using the clay-to-silt ratio (Fig. 5). The correlation between maximum eroded depth and maximum wave-current stress is 0.89 (with WMS removed). In the deep basins where stress is small, erosion is predicted to be zero at stations nine and NWB; and near-zero at WJB. The low erosion at WMS reflects the sandy sediments there. The mean eroded depth at GM and EMS reflects the constant resuspension by tidal currents.

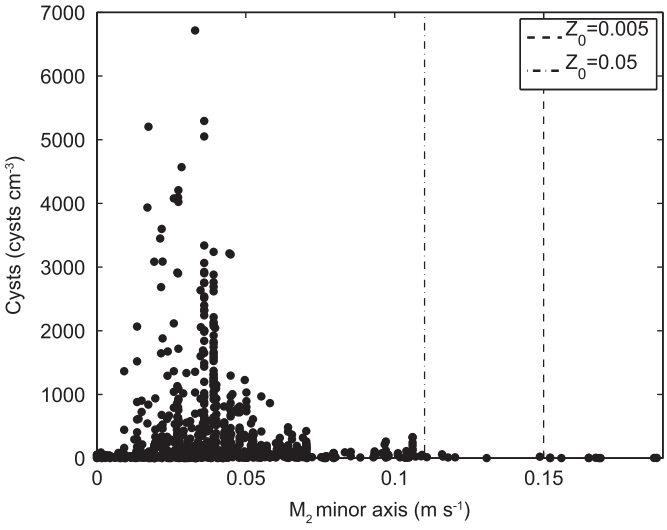

Fig. 11. Cyst concentration in 0–1 cm for all cyst-map cruises vs. amplitude of the minor axis of the M_2 tidal ellipse (a measure of the minimum near-bottom tidal current). The vertical lines indicate a bottom stress of 0.05 Pa for a bottom roughness (z_0) of 0.005 and 0.05 m.

The UGEMS system provided an opportunity to estimate cyst abundance in the material mostly likely to be suspended. Concentration, in cysts kg^{-1}, was determined directly from the UGEMS analysis and in the 0–3 cm interval of the Craib cores using the measured solids mass fraction and measured cysts cm^{-3}. The concentration of cysts in the eroded sediment was higher than the concentration in the 0–3 cm interval at some stations (by a factor of 15.4, 1.5, 3.0, and 1.6 at WMS, EMS, CMS, and CMSB, respectively) and lower at others (by a factor 0.6, 0.4, and 0.8 at NWB, WJB, and GM, respectively). The near-surface enrichment at CMSB is qualitatively consistent with model predictions that recently settled cysts in the central Maine seedbed remain at the sediment surface for at least a few months (Shull et al., 2014). However, the concentrations were determined from separate cores taken at slightly different locations, so differences caused by local spatial variability cannot be ruled out. In addition, UGEMS might preferentially remove cysts in sandy sediments (for example WMS).

The combination of increasing critical erosion stress with sediment depth, varying critical stresses for each sediment class, swelling, consolidation, the time-varying magnitudes of deposition and erosion, and the vertical velocity in the water column predicted by FVCOM result in a complex interaction between the processes that goes beyond the intuitive relation of larger wave-current stress resulting in larger erosion. In addition, the sediment response predicted by the model is sensitive to the initial conditions; the mass-eroded profile in the model (Fig. 4) is assumed to be the average state, but in fact reflects the history of sediment processes prior to sampling. For a given bottom stress, the particle settling velocities have a strong impact on the duration and vertical extent of resuspension; the chosen speeds for mud (0.1 mm s^{-1}) and sand (8 mm s^{-1}) might be increased by flocculation and pelletization, factors that are not included in the model. A faster settling speed would result in the suspended mass settling more quickly.

The analysis of inter-annual variability of bottom stress indicates that wave-driven (and, by extension, storm-driven) processes for 2010–2011 are typical for the region and that resuspension and mobility of sediment and cysts are probable during most years. The contribution to stress from tidal currents will not show significant inter-annual variability (except for the 18.6-year nodal modulations, see below); therefore these results indicate that the mobility and potential for resuspension indicated by the analysis of 2010–2011 are not anomalous. The range in the number of events in winter (12–23 at 24 m and 0–11 at 83 m over a 6-month period) and spring (1–8 at 24 m and 0–2 at 83 m in a 2-month period) (Table 3) suggests there could be significant inter-annual differences in resuspension along the Maine coast.

Several processes that are potentially capable of affecting sediment resuspension are not included in these simulations. Resuspension of sediment by large-amplitude internal waves, common in nearby coastal environments (Butman et al., 2006), would be expected in late summer when water-column stratification is strongest. Effects would occur in regions along the coast and around topographic highs as the internal waves shoal. Variability in the tidal currents at the 18.6-year nodal period, estimated at about 4% (Godin, 1972; Greenberg et al., 2012) (approximately 7% in stress), could modulate the stress characteristics, resulting in peak tidal stress during 1997 and minimal values in 2005–2006. Deposition might be reduced during periods of stronger tides and enhanced during periods of weaker tides, affecting the inventory of cysts. It is of note that 1997 falls in a decadal interval or regime of low shellfish toxicity and presumed low cyst abundance in the Gulf of Maine, whereas 2005 and 2006 fall within a regime with much higher toxicity, and demonstrably higher cyst concentrations (Anderson et al., 2014a; Kleindinst et al., 2014).

In addition to sediment and cyst resuspension attributed to waves and currents, resuspension of the bottom sediments may also be caused by bottom trawling (Pilskaln et al., 1998). Churchill (1989) reported that as much as 0.04 m of surficial sediment might be reworked during passage of otter trawl doors over a muddy bottom. Present estimates of bottom trawling from the Swept Area Seabed Impact (SASI) model (New England Fishery Management Council, 2011) for 2008–2010 data shows the seafloor was trawled

in excess of 5 times per year in eastern Wilkinson Basin, over Jeffreys Ledge and Stellwagen Bank, and in some locations along the coast (S. Lucey, personal communication). There was little trawling in the mid-coast Maine seed bed south of Penobscot Bay. Given the estimates that less than a few mm of sediment are reworked by waves and currents, bottom trawling appears likely to be an important cause of sediment resuspension in some areas of the Maine coast and in the eastern Wilkinson Basin.

There is a well-defined near-bottom nepheloid layer (BNL) in Wilkinson and Jordan Basins (Spinrad, 1986; Townsend et al., 1992; Pilskaln et al., 1998, 2014a, 2014b). Sediment trap flux observations in Jordan Basin at a location in water 280 m deep are not inconsistent with a local balance between input from the upper water column and local resuspension (Pilskaln et al., 2014a). The 1-dimensional model used here predicts minor and infrequent resuspension at WJB (Fig. 7), a result of near-bottom tidal currents less than about 0.15 m s^{-1} and water too deep to be affected by waves. Station WJB, however, is located on the western side of Jordan Basin and the estimated wave-current bottom stress exceeded 5% of the time increases to between 0.1 and 0.3 Pa on the eastern side of the basin, and continues to increase eastward into the Bay of Fundy (Fig. 6). Although no erodibility measurements were made in eastern Jordan Basin, the estimated stresses there are likely sufficient to resuspend sediment that could contribute to the BNL. Indeed, beam attenuation observations suggest resuspension in eastern Jordan Basin, continuing into the Bay of Fundy (Pilskaln et al., 2014b); this resuspended material could be transported throughout the basin by the Jordan Basin gyre (Brooks, 1985; Pettigrew et al., 1998; Aretxabaleta et al., 2014). In Wilkinson Basin, stress exceeded 5% of the time was less than 0.05 Pa in the northern part of the basin, increasing to 0.05–0.1 Pa toward the south. The model did not predict resuspension at either NWB or station nine in southern Wilkinson Basin (Figs. 9 and 10), suggesting that sediment in the BNL in Wilkinson Basin is not from local flow-induced resuspension. Several processes not included in the model could contribute sediment to the observed persistent BNL in the basins: (1) local resuspension by trawling (especially in eastern Wilkinson Basin) or benthic organisms; (2) resuspension in shallower water (by storm-driven currents, surface waves, tides, or internal waves) and subsequent transport to the deeper basins; (3) and settling of biogenic or terrigenous sediment from surface waters. Sediment delivered to the bottom boundary layer via any of these mechanisms could be maintained in suspension indefinitely in a BNL if vertical mixing is sufficient to balance (potentially very slow) settling rates. The relative contributions of these processes to the formation and maintenance of the BNL and the sensitivity of resuspension to model parameters could be explored using a full 3-dimensional circulation and sediment transport model.

The effect of resuspension on cysts depends on their concentration in the mobile layer of the bed, estimated here to be about 1 mm thick. Using a bed model with non-local mixing based on the abundance and depth distribution of benthic deposit feeders at 168 m in the mid-coast Maine cyst seedbed, Shull et al. (2014) suggest that some recently deposited cysts remain at the sediment surface for several months; the surface concentration decreases by about 80% after about 3 months as cysts are mixed downward. Keafer et al. (1992), using a constant mixing rate model based on observations at 160 m in the western Gulf of Maine, suggest that mixing would reduce the concentration of cysts at the sediment surface by about 50% after 6 months. Thus the amount of cysts available for resuspension is highest immediately following deposition and decreases with time, but both studies suggest significant cyst concentrations remain in the mobile layer after a few months.

The answer to the question 'is resuspension a mechanism for cysts to enter the water column in spring' is that there are some years when cysts may be resuspended into the water column at that time. Typically, less than 1 mm of sediment was predicted to be eroded by the events of 2010–2011. Shull et al. (2014) suggests that about 20% of the cysts deposited in fall might remain in the upper mm of sediment after about 3 months. In spring, a single storm event could resuspend most of these cysts in a few hours. For sediment with 1000 cysts cm^{-3} mixing the upper mm throughout a water depth of 100 m would result in a concentration of about 10^4 cysts m^{-3}. If cysts with a high germination potential (April through June) (Anderson et al., 2005) are resuspended into conditions more favorable for growth (primarily increased light and warmer temperatures), the resuspension could affect the evolution of the bloom. The number of resuspension events in spring varied from 0 to 2 at 83 m and 1–8 at 24 m (Table 3), and thus resuspension of cysts might occur in some years, and not at all in others. Kirn et al. (2005) reached similar conclusions but predicted more frequent resuspension events using a critical shear stress of 0.02 Pa (less than the 0.05 Pa used here) and stress calculated using a bottom roughness of 1 cm (probably an overestimate for the grain-sized based skin friction used for sediment transport calculation).

Downwelling-favorable winds (from the north or northeast) drive currents that carry *A. fundyense* cells southwestward and compress them in a plume along the coast (Franks and Anderson, 1992; Hetland et al., 2003; Anderson et al., 2005a, 2005b). This shoreward and alongshore transport of established populations of cells has typically been the role attributed to these large storms, but the effect of cyst resuspension by strong wind events in the spring as a means to inoculate or augment motile populations has not been considered. Butman et al. (2008) show the largest wave stress events in the western Gulf of Maine are associated with northeasters, and thus in spring these storms might introduce cysts into the water column that quickly germinate to produce motile cells, thereby contributing to the bloom inoculum.

One of the strongest *A. fundyense* blooms in the Gulf of Maine occurred in spring 2005 (Anderson et al., 2005; He et al., 2008; Kleindinst et al., 2014), shortly after and during two of the strongest nor'easters recorded between 1990 and 2006, ranked by wave bottom stress calculated at 30 m water depth in Massachusetts Bay (7 May and 22 May 2005; Butman et al., 2008). Indeed, total mass flux (TMF) to sediment traps at depths of 75 m and 135 m at a 150-m deep site in the central Maine seed bed increased during the May storms, attributed to organic particulates from the spring bloom as well as fine-sediment resuspension input generated by the May storms (Pilskaln et al., 2014a). The largest TMF and cyst flux to a trap at 255 m in Jordan Basin at 280 m water depth was in the sampling interval that included the 7 May storm, possibly reflecting sediment and cyst resuspension on the shelf and advection to the deep basin (Pilskaln et al., 2014a). These trap observations are consistent with model predictions of increased sediment and cyst concentrations in the water column during major storms. Another major northeast storm on 23 October 2005 (Butman et al., 2008) occurred between sediment trap deployments and thus effects are not reflected in the observations (C. Pilskaln, personal communication). Simulations of the 2005 bloom have been run to test sensitivity to cyst distribution, river inflow, and winds (He et al., 2008), but did not include cyst resuspension. Spring 2005 would be a good period to explore the effect of resuspension events on the progression of the bloom.

The answer to the question 'can resuspension and transport in winter reshape the autumn cyst distribution,' is that episodic resuspension of cysts in the upper 1 mm of sediment can occur, and that the location and frequency depends on the mix of processes causing resuspension (Figs. 6 and 9). The bed models (Shull et al., 2014; Keafer et al., 1992) suggest that resuspension events that occur soon after deposition, when cysts are at the sediment surface, could resuspend most of the recently-deposited cysts. The concentration of cysts in the

mobile layer would decrease over time as these cysts are mixed downward. Cysts with fall velocities similar to the clay particles modeled here (0.1 mm s^{-1}) (Anderson et al., 1985) could remain in suspension for several days (for example at CMSB, Fig. 8). In simulations of trajectories of resuspended particles at CMSB for 2010–2011, about 18% of the resuspended material was transported in excess of 20 km from the source and about 5% in excess of 50 km from the source (Aretxabaleta et al., 2014). The effect of resuspension on the surface distribution over the winter depends on the concentration of cysts in the mobile layer; mixing in the sediment column; the number, intensity, and timing of resuspension events; and the distance the cysts are transported before re-depositing on the sea floor. The effect of these variables on the cysts in the upper cm, those most likely to contribute to the spring bloom, cannot be assessed with the data presented here, but could be investigated using a 3-dimensional circulation and sediment transport model. However, resuspension and transport are unlikely to change spatial patterns in the total inventory of cysts that extends to 15 cm or more below the sediment surface.

5. Summary

Sediment erodibility observations, simulations of sediment resuspension, and seasonal calculations of wave-current bottom stress suggest that sediment and cyst resuspension and subsequent transport could be significant for *A. fundyense* cyst dynamics in the Gulf of Maine. The observations and model results suggest that a millimeter or so of sediment and associated cysts may be mobilized in both winter and spring, and that the frequency of resuspension will vary interannually. Field observations of sediment resuspension are needed to further assess model predictions. Depending on cyst concentration, location in the sediment, and the resulting vertical distribution in the water column, these events could result in a concentration of at least 10^4 cysts m^{-3}. The effect of resuspension on the distribution of cysts in near-surface sediment depends on the concentration in the mobile layer; mixing in the sediment column; the number, intensity, and timing of resuspension events; and the distance the cysts are transported before re-depositing on the sea floor. Resuspension and transport are unlikely to affect spatial patterns in the total inventory of cysts that extends to at least 15 cm below the sediment surface. In some years, resuspension events could episodically introduce cysts into the water column in spring, where germination and growth are likely to be facilitated by light. In this instance, spring northeasters might contribute to the bloom inoculum, while also creating down-welling conditions that bring the resulting motile cell populations to shore. In prior studies, only the latter effect was attributed to these storms. The sediment model simulated complex interactions between the time-history of the stress, properties of the sediment bed (swelling), and water column (mixing, downwelling) that go beyond the intuitive relation of larger wave–current stress resulting in larger erosion. The quantitative effect that resuspension and transport might have on the growth and spread of the *A. fundyense* population in a particular year, which is a complex interaction between biological and physical processes, remains to be determined.

Acknowledgments

We thank the officers and crews of RV *Endeavor* and *Oceanus* for skillful assistance in sediment sampling operations. Jon Borden, Sandy Baldwin, and Kate McMullen (USGS) assisted in core collection and sample processing at sea, and Kate McMullen did all the sediment texture analysis. Kerry Norton (WHOI) assisted in collection of the Craib cores and counted the UGEMS samples for cyst concentrations. Sean Lucey, NOAA Northeast Fisheries Science Center Ecosystem Assessment Program, provided the SASI bottom trawling estimates. Changsheng Chen (UMASS Dartmouth) ran the FVCOM forecasts that are provided online at the archive http://www.smast.umassd.edu:8080/thredds/archives.html. Three anonymous reviewers and Page Valentine provided very thorough and helpful reviews of the manuscript. D. Shull provided insight and additional runs of a sediment bed model to help clarify the role of mixing. C. Pilskaln provided a helpful review and insight on sediment trap results. D. McGillicuddy provided several careful and constructive reviews. Research support to Donald M. Anderson and Bruce A. Keafer provided through the Woods Hole Center for Oceans and Human Health; National Science Foundation Grants OCE-0430724 and OCE-0911031; and National Institute of Environmental Health Sciences Grant 1-P50-ES012742-01; the ECOHAB Grant program through NOAA Grants NA06NOS4780245 and A09NOS4780193; the MERHAB Grant program through NOAA Grant NA11NOS4780025; and the PCMHAB Grant program through NOAA Grant NA11NOS4780023. This is ECOHAB contribution 746, MERHAB contribution 169, and PCMHAB contribution 8. Research support to all other authors was provided by U.S. Geological Survey.

Any use of trade, firm, or product names is for descriptive purposes only and does not imply endorsement by the U.S. Government.

References

Anderson, D.M., 1998. Physiology and bloom dynamics of toxic Alexandrium species, with emphasis on life cycle transitions. In: Anderson, D.M., Cembella, A.D., Hallegraeff, G.M. (Eds.), The Physiological Ecology of Harmful Algal Blooms. Springer-Verlag, Heidelberg, pp. 29–48.

Anderson, D.M., 1980. The effects of temperature conditioning on the development and germination of *Gonyaulax tamarensis* (*Dinophyceae*) hypnozygotes. J. Phycol. 16, 166–172.

Anderson, D.M., Couture, D., Keafer, B.A., Kleindinst, J.L., McGillicuddy Jr., D.J., Martin, J.L., Hickey, J.M., 2014a. Understanding interannual, decadal level variability in PSP toxicity in the Gulf of Maine: the HAB Index and *Alexandrium fundyense* cyst abundance. Deep-Sea Res. II Top. Stud. Oceanogr. 103, 264–276.

Anderson, D.M., Fukuyo, Y., Matsuoka, K., 2003. Cyst methodologies. In: Hallegraeff, G.M., Anderson, D.M., Cembella, A.D. (Eds.), Manual on Harmful Marine Microalgae, Monographs on Oceanographic Methodology, 11. UNESCO, Paris, pp. 165–190.

Anderson, D.M., Keafer, B.A., 1987. An endogenous annual clock in the toxic marine dinoflagellate *Gonyaulax tamarensis*. Nature 325, 616–617.

Anderson, D.M., Keafer, B.A., Geyer, W.R., Signell, R.P., Loder, T.C., 2005. Toxic *Alexandrium* blooms in the western Gulf of Maine. The plume advection hypothesis revisited. Limnol. Oceanogr. 50 (1), 328–345.

Anderson, D.M., Keafer, B.A., Kleindinst, J.L., McGillicuddy Jr., D.J., Martin, J.L., Norton, K., Pilskaln, C.H., Smith, J.L., Sherwood, C.R., Butman, B., 2014b. *Alexandrium fundyense* cysts in the Gulf of Maine: long-term time series of abundance and distribution, and linkages to past and future blooms. Deep-Sea Res. II Top. Stud. Oceanogr. 103, 6–26.

Anderson, D.M., Keafer, B.A., McGillicuddy Jr., D.J., Mickelson, M.J., Keay, K.E., Libby, P.S., Manning, J.P., Mayo, C.A., Whittaker, D.K., Hickey, J.M., He, Ruoying, Lynch, D.R., Smith, K.W., 2005b. Initial observations of the 2005 *Alexandrium fundyense* bloom in southern New England: General patterns and mechanisms. Deep-Sea Res. II Top. Stud. Oceanogr. 52, 2856–2876.

Anderson, D.M., Lively, J.J., Reardon, E.M., Price, C.A., 1985. Sinking characteristics of dinoflagellate cysts. Limnol. Oceanogr. 30 (5), 1000–1009.

Anderson, D.M., Stock, C.A., Keafer, B.A., Nelson, A.B., McGillicuddy Jr., D.J., Keller, M., Thompson, B., Matrai, P.A., Martin, J., 2005c. *Alexandrium fundyense* cyst dynamics in the Gulf of Maine. Deep-Sea Res. II Top. Stud. Oceanogr. 52, 2522–2542.

Anderson, D.M., Taylor, C.D., Armbrust, E.V., 1987. The effects of darkness and anaerobiosis on dinoflagellate cyst germination. Limnol. Oceanogr. 32, 340–351.

Anderson, D.M., Wall, D., 1978. Potential importance of benthic cysts of *Gonyaulax tamarensis* and *G. excavata* in initiating toxic dinoflagellate blooms. J. Phycol. 14, 224–234.

Aretxabaleta, A.L., Butman, B., Signell, R.P., Dalyander, P.S., Sherwood, C.R., McGillicuddy Jr., D.J., 2014. Near-bottom circulation and dispersion of sediment containing *Alexandrium fundyense* cysts in the Gulf of Maine during 2010–2011. Deep-Sea Res. II Top. Stud. Oceanogr. 103, 96–111.

Aretxabaleta, A.L., McGillicuddy Jr., D.J., Smith, K.W., Lynch, D.R., 2008. Model simulations of the Bay of Fundy Gyre: 1. Climatological results. J. Geophys. Res. 113, C10027.

Barnhardt, W.A., Kelley, J.T., Dickson, S.M., Belknap, D.F., Kelley, A.R., 1996. Surficial geology of the Maine inner continental shelf (map series): Maine Geological Survey, Natural Resources Information and Mapping Center, scale 1:100,000. Available from: ⟨http://www.maine.gov/doc/nrimc/mgs/pubs/online/ics/ics.htm⟩.

Bever, A.J., Harris, C.K., Sherwood, C.R., Signell, R.P., 2009. Deposition and flux of sediment from the Po River, Italy: an idealized and wintertime numerical modeling study. Mar. Geol. 260 (1), 69–80.

Bothner, M.H., Gill, P.W., Boothman, W.S., Taylor, B.B., Karl, H.A., 1997. Chemical and Textural Characteristics of Sediments at an EPA Reference Site for Dredged Material on the Continental Slope SW of the Farallon Islands. U.S. Geological Survey Open-File Report 97–87, 51p. Available from: ⟨http://pubs.usgs.gov/of/1997/0087/report.pdf⟩.

Brooks, D.A., 1985. Vernal circulation in the Gulf of Maine. J. Geophys. Res. 90 (C3), 4687–4706.

Butman, B., Alexander, P.S., Scotti, A., Beardsley, R.C., Anderson, S.P., 2006. Large internal waves in Massachusetts Bay transport sediments offshore. Cont. Shelf Res. 26/17–18, 2029–2049, http://dx.doi.org/10.1016/j.csr.2006.07.022.

Butman, B., Sherwood, C.R., Dalyander, P.S., 2008. Northeast storms ranked by wind stress and wave-generated bottom stress observed in Massachusetts Bay, 1990–2006. Cont. Shelf Res. 28, 1231–1245, http://dx.doi.org/10.1016/j.csr.2008.02.010.

Chen, C., Lui, H., Beardsley, R.C., 2003. An unstructured, finite-volume, three-dimensional, primitive equation ocean model: application to coastal ocean and estuaries. J. Atmos. Ocean. Technol. 20, 159–186.

Craib, J.S., 1965. A sampler for taking short undisturbed marine cores. J. Cons. 30, 34–39.

Churchill, J.H., 1989. The effect of commercial trawling on sediment resuspension and transport over the Middle Atlantic Bight continental shelf. Cont. Shelf Res. 9, 841–864.

Dalyander, P. Soupy, Butman, B., Sherwood, C.R., Signell, R. P., 2012. Documentation of the U.S. Geological Survey Sea Floor Stress and Sediment Mobility Database. U.S. Geological Survey Open File Report 2012–1137, 20p. Available from: ⟨http://pubs.usgs.gov/of/2012/1137⟩.

Dalyander, P. Soupy, Butman, B., Sherwood, C.R., Signell, R.P., Wilkin, J.L., 2013. Characterizing wave- and current-induced bottom shear stress: U.S. middle Atlantic continental shelf. Cont. Shelf Res. 52, 73–86.

Dickhudt, P.J., Friedrichs, C.T., Sanford, L.P., 2011. Mud matrix solids fraction and bed erodibility in the York River estuary, USA, and other muddy environments. Cont. Shelf Res. 31 (10, Suppl. 1), S3–S13.

Dietrich, W.E., 1982. Settling velocities of natural particles. Water Resour. Res. 18 (6), 1615–1626.

Fader, G.B., King, L.H., MacLean, B., 1977. Surficial Geology of the eastern Gulf of Maine and Bay of Fundy. Marine Sciences Paper 19, 23p. (also Geological Survey of Canada Paper 76-17).

Franks, P.J.S., Anderson, D.M., 1992. Alongshore transport of a toxic phytoplankton bloom in a buoyancy current: *Alexandrium tamarensis* in the Gulf of Maine. Mar. Biol. 112, 153–164.

Godin, G., 1972. Analysis of Tides. University of Toronto Press, Toronto and Buffalo.

Greenberg, D.A., 1979. A numerical model investigation of tidal phenomena in the Bay of Fundy and Gulf of Maine. Mar. Geod. 2, 161–187.

Greenberg, D.A., Blanchard, W., Smith, B., Barrow, E., 2012. Climate change, mean sea level and high tides in the Bay of Fundy. Atmos. Ocean 50 (3), 261–276.

Gust, G., Mueller, V., 1997. Interfacial hydrodynamics and entrainment functions of currently used erosion devices. In: Burt, N., Parker, R., Watts, J. (Eds.), Cohesive sediments. Wallingford, U.K., pp. 149–174.

He, R., McGillicuddy, D.J., Anderson, D.M, Keafer, B.A., 2008. Historic 2005 toxic bloom of *Alexandrium fundyense* in the western Gulf of Maine: 2. Coupled biophysical modeling. J. Geophys. Res. Oceans 113, C07040, http://dx.doi.org/10.1029/2007JC004602.

Hetland, R.D., McGillicuddy, D.J., Signell, R.P., 2003. Cross-frontal entrainment of plankton into a buoyant plume: the frog-tongue hypothesis. J. Mar. Res. 60, 763–777.

Hill, P.S., Milligan, T.G., Geyer, W.R., 2000. Controls on effective settling velocity of suspended sediment in the Eel River flood plume. Cont. Shelf Res. 20 (16), 2095–2111.

Holthuijsen, L.H., Booij, N., Ris, R.C., 1993. A spectral wave model for the coastal zone. In: Proceedings of the 2nd International Symposium on Ocean Wave Measurement and Analysis, pp. 630–641.

Keafer, B.A., Buesseler, K.O., Anderson, D.M., 1992. Burial of living dinoflagellate cysts in estuarine and nearshore sediments. Mar. Micropaleontol. 20, 147–161.

Kirn, S.L., Townsend, D.W., Pettigrew, N.R., 2005. Suspended *Alexandrium* spp. hypnozygote cysts in the Gulf of Maine. Deep-Sea Res. 52, 2543–2559.

Kleindinst, J.L., Anderson, D.M., McGillicuddy Jr., D.J., Stumpf, R.P., Fisher, K.M., Darcie Couture, D., Hickey, J.M., Nash, C., 2014. Categorizing the severity of paralytic shellfish poisoning outbreaks in the Gulf of Maine for forecasting and management. Deep-Sea Res. II Top. Stud. Oceanogr. 103, 277–287.

Law, B.A., Hill, P.S., Milligan, T.G., Curran, K.J., Wiberg, P.L., Wheatcroft, R.A., 2008. Size sorting of fine-grained sediments during erosion: Results from the western Gulf of Lions. Cont. Shelf Res. 28, 1935–1946.

Le Hir, P., Cayocca, F., Waeles, B., 2011. Dynamics of sand and mud mixtures: a multiprocess-based modelling strategy. Cont. Shelf Res. 31 (Suppl. 10), S135–S149.

Li, Y., He, R., McGillicuddy, D.J., Anderson, D.M., Keafer, B.A., 2009. Investigation of the 2006 *Alexandrium fundyense* bloom in the Gulf of Maine: in-situ observations and numerical modeling. Cont. Shelf Res. 29, 2069–2082.

Lilly, E.L., Halanych, K.M., Anderson, D.M., 2007. Species boundaries and global biogeography of the *Alexandrium tamarense* complex (Dinophyceae). J. Phycol. 43, 1329–1338.

Lynch, D.R., Naimie, C.E., 1993. The M2 Tide and its residual on the outer banks of the Gulf of Maine. J. Phys. Oceanogr. 23, 2222–2253.

Maa, J.P.-Y., Wright, L.D., Lee, C.H., Shannon, T.W., 1993. VIMS Sea Carousel: a field instrument for studying sediment transport. Mar. Geol. 115, 271–287.

Madsen, O.S., 1994. Spectral wave-current bottom boundary layer flows. In: Proceedings of the 24th International Conference on Coastal Engineering, pp. 384–398.

Martin, J.L., LeGresley, M.M., Hanke, A.R., 2014. Thirty years—*Alexandrium fundyense* cyst, bloom dynamics and shellfish toxicity in the Bay of Fundy, eastern Canada. Deep-Sea Res. II Top. Stud. Oceanogr. 103, 27–39.

McGillicuddy, D.J., Anderson, D.M., Lynch, D.R., Townsend, D.W., 2005. Mechanisms regulating the large-scale seasonal fluctuations in *Alexandrium fundyense* populations in the Gulf of Maine; Results from a physical–biological model. Deep-Sea Res. II Top. Stud. Oceanogr. 52, 2698–2714.

McGillicuddy Jr., D.J., Townsend, D.W., He, R., Keafer, B.A., Kleindinst, J.L., Li, Y., Manning, J.P., Mountain, D.G., Thomas, M.A., Anderson, D.M., 2011. Suppression of the 2010 *Alexandrium fundyense* bloom by changes in physical, biological, and chemical properties of the Gulf of Maine. Limnol. Oceanogr. 56 (6), 2411–2426.

McMullen, K.Y., Paskevich, V.F., Poppe, L.J., 2011. GIS data catalog (version 2.2). In: Poppe, L.J., Williams, S.J., Paskevich, V.F. (Eds.), 2005, USGS East-Coast Sediment Analysis: Procedures, Database, and GIS data. U.S. Geological Survey Open-File Report 2005-1001. Available from: ⟨http://woodshole.er.usgs.gov/openfile/of2005-1001/htmldocs/datacatalog.htm⟩.

New England Fishery Management Council, 2011. The Swept Area Seabed Impact (SASI) model: A Tool for Analyzing the Effects of Fishing on Essential Fish Habitat. New England Fishery Management Council, 303p. Available from: ⟨http://www.nefmc.org/habitat/sasi_info/110121_SASI_Document.pdf⟩.

Pawlowicz, R., Beardsley, R.C., Lentz, S., 2002. Classical tidal harmonic analysis including error estimates in MATLAB using TTIDE. Comput. Geosci. 28, 929–937.

Pettigrew, N.R., Townsend, D.W., Xue, H., Wallinga, J.P., Brickley, P.J., Hetland, R.D., 1998. Observations of the Eastern Maine Coastal Current and its offshore extensions in 1994. J. Geophys. Res. 103 (C13), 30623–30639.

Pilskaln, C.H., Churchill, J.M., Mayer, L.M., 1998. Resuspension of sediment by bottom trawling in the Gulf of Maine and potential geochemical consequences. Conserv. Biol. 12 (6), 1223–1229.

Pilskaln, C.H., Anderson, D.M., McGillicuddy, D.J., Keafer, B.A., Hayashi, K., Norton, K., 2014a. Spatial and temporal variability of Alexandrium cyst fluxes in the Gulf of Maine: relationship to seasonal particle export and resuspension. Deep-Sea Res. II 103, 40–54.

Pilskaln, C.H., Hayashi, K., Keafer, B.A., Anderson, D.M., McGillicuddy, D.J., 2014b. Benthic nepheloid layers in the Gulf of Maine and *Alexandrium* cyst inventories. Deep-Sea Res. II Top. Stud. Oceanogr. 103, 55–65.

Poppe, L.J., Eliason, A.H., Fredericks, J.J., Rendigs, R.R., Blackwood, D., Polloni, C.F., 2000. Grain-size analysis of marine sediments—methodology and data processing. In: USGS East-Coast Sediment Analysis: Procedures, Database and Georeferenced Displays. U.S. Geological Survey Open-File Report 00-358 (Chapter 1). Available from: ⟨http://pubs.usgs.gov/of/2000/of00-358/⟩.

Rinehimer, J.P., Harris, C.K., Sherwood, C.R., Sanford, L.P., 2008. Estimating cohesive sediment erosion and consolidation in a muddy, tidally-dominated environment: model behavior and sensitivity. Estuarine and Coastal Modeling, 2007. American Society of Civil Engineers, Reston, VA, pp. 819–838, ⟨10.1061/40990(324)44⟩.

Sanford, L.P., 2006. Uncertainties in sediment erodibility estimates due to a lack of standards for experimental protocols and data interpretation. Integr. Environ. Assess. Manage. 2 (1), 29–34.

Sanford, L.P., 2008. Modeling a dynamically varying mixed sediment bed with erosion, deposition, bioturbation, consolidation, and armoring. Comput. Geosci. 34, 1263–1283.

Sanford, L.P., Maa, J.P.Y., 2001. A unified erosion formulation for fine sediments. Mar. Geol. 179, 9–23.

Shull, D.H., Kremp, A., Mayer, L.M., 2014. Bioturbation, germination and deposition of *Alexandrium fundyense* cysts in the Gulf of Maine. Deep-Sea Res. II Top. Stud. Oceanogr. 103, 66–78.

Shaw, J., Todd, B.J., Li, M.Z., 2012. Seascapes, Bay of Fundy, offshore Nova Scotia/New Brunswick. Geological Survey of Canada, Open file 7028, scale 1:350,000.

Stevens, A.W., Wheatcroft, R.A., Wiberg, P.L., 2007. Seabed properties and sediment erodibility along the western Adriatic margin, Italy. Cont. Shelf Res. 27, 400–416.

Soulsby, R.L., 1997. Dynamics of Marine Sands. Thomas Telford, London. (249pp.).

Spinrad, R.W., 1986. An optical study of the water masses of the Gulf of Maine. J. Geophys. Res. 91, 1007–1018.

Stock, C.A., McGillicuddy, D.J., Solow, A.R., Anderson, D.M., 2005. Evaluating hypotheses for the initiation and development of *Alexandrium fundyense* blooms in the western Gulf of Maine using a coupled physical–biological model. Deep-Sea Res. II 52, 2715–2744.

Todd, B.J., Shaw, J., Parrott, D.R., Hughes Clarke, J.E., Cartwright, D., Hayward, S.E., 2011. Backscatter strength and shaded seafloor relief, Bay of Fundy, Sheet 4, offshore Nova Scotia-New Brunswick, Canada—United States of America; Geological Survey of Canada, Open File 7021, scale 1:50,000, http://dx.doi.org/10.4095/289511.

Townsend, D.W., Mayer, L.M., Dortch, Q., Spinrad, R.W., 1992. Vertical structure and biological activity in the bottom nepheloid layer of the Gulf of Maine. Cont. Shelf Res. 12, 367–387.

U.S. Geological Survey, 2012. U.S. Geological Survey Sea Floor Stress and Sediment Mobility Database. Available from: ⟨http://woodshole.er.usgs.gov/project-pages/mobility/index.html⟩.

van Rijn, L.C., 2007. Unified view of sediment transport by currents and waves. I: initiation of motion, bed roughness, and bed-load transport. J. Hydraul. Eng. 133.6, 649–667.

Warner, J.C., Sherwood, C.R., Signell, R.P., Harris, C., Arango, H., 2008. Development of a three-dimensional, regional, coupled wave, current, and sediment-transport model. Comput. Geosci. 34 (10), 1284–1306.

Xu, K., Harris, C.K., Hetland, R.D., Kaihatu, J.M., 2011. Dispersal of Mississippi and Atchafalaya sediment on the Texas–Louisiana shelf: model estimates for the year 1993. Cont. Shelf Res. 31 (15), 1558–1575.

Yamaguchi, M., Itakura, S., Imai, I., Ishida, Y., 1995. A rapid and precise technique for enumeration of resting cysts of *Alexandrium* spp. (Dinophyceae) in natural sediments. Phycologia 34, 207–214.